SDIO GBL SETA FY 1989 FINAL REPORT

VOLUME 2

Task 3 - Laser Devices and Systems

SAIC TR 89/1574

Science Applications International Corporation

An Employee-Owned Company

SDIO GBL SETA FY 1989 FINAL REPORT

VOLUME 2

Task 3 - Laser Devices and Systems

SAIC TR 89/1574

TO

W. J. SCHAFFER ASSOCIATES, INC.
1901 North Fort Myer Drive, Suite 800
Arlington, VA 22209-1681

CONTRACT
SDIO84-88-C-0057

SUBCONTRACT
SC-88W-34-003

WITH

SDIO/T/DE
The Pentagon
Washington, D. C. 20301-7100

PREPARED BY

SCIENCE APPLICATIONS INTERNATIONAL CORPORATION
1040 Waltham Street, Lexington, MA 02173 - (617) 863-5173
1519 Johnson Ferry Road, Suite 300, Marietta, GA 30062 - (404) 973-8935

Accession Number: 2186

Publication Date: Sep 01, 1989

Title: SDIO GBL SETA FY 1989 Final Report, Vol. 2: Task 3 - Laser Devices and Systems

Personal Author: Mani, S.A.; Gebhardt, F.G.; Hills, L.S.; Long, J.E.

Corporate Author Or Publisher: Science Applications International Corp., 1040 Waltham St., Lexington, Report Number: SAIC TR-89/1574

Descriptors, Keywords: GBFEL TIE FEL Superconductor Accelerator Linac RF Induction Amplifier Wiggler GBL Code Model Simulation DEW Cryogenics Optics Cavity Klystron

Pages: 053

Cataloged Date: Jun 13, 1990

Contract Number: SDIO84-88-C-0057

Document Type: HC

Number of Copies In Library: 000001

Record ID: 21104

UNCLASSIFIED
SECURITY CLASSIFICATION OF THIS PAGE

REPORT DOCUMENTATION PAGE

Form Approved
OMB No. 0704-0188
Exp. Date: Jun 30, 1986

1a. REPORT SECURITY CLASSIFICATION
UNCLASSIFIED

1b. RESTRICTIVE MARKINGS
NONE

2a. SECURITY CLASSIFICATION AUTHORITY

2b. DECLASSIFICATION / DOWNGRADING SCHEDULE

3. DISTRIBUTION / AVAILABILITY OF REPORT

4. PERFORMING ORGANIZATION REPORT NUMBER(S)
SAIC TR 89/1574

5. MONITORING ORGANIZATION REPORT NUMBER(S)

6a. NAME OF PERFORMING ORGANIZATION
Science Applications International Corporation

6b. OFFICE SYMBOL (If applicable)

7a. NAME OF MONITORING ORGANIZATION

6c. ADDRESS (City, State, and ZIP Code)
1040 Waltham Street
Lexington, MA 02173

7b. ADDRESS (City, State, and ZIP Code)

8a. NAME OF FUNDING / SPONSORING ORGANIZATION
W.J. SCHAFFER Associated

8b. OFFICE SYMBOL (If applicable)

9. PROCUREMENT INSTRUMENT IDENTIFICATION NUMBER

8c. ADDRESS (City, State, and ZIP Code)
1901 North Fort Myer Drive, Suite 800
Arlington, VA 22209-1681

10. SOURCE OF FUNDING NUMBERS

PROGRAM ELEMENT NO.	PROJECT NO.	TASK NO.	WORK UNIT ACCESSION NO.

11. TITLE (Include Security Classification)
(U) SDIO GBL SETA FY 1989 FINAL REPORT -- VOLUME 2 -- Task 3 - Laser Devices and Systems

12. PERSONAL AUTHOR(S)
Siva A. Mani, Frederick G. Gebhardt, L. Scott Hills, Jerry E. Long

13a. TYPE OF REPORT	13b. TIME COVERED	14. DATE OF REPORT (Year, Month, Day)	15. PAGE COUNT
Final	FROM 10/24/88 TO 10/23/89	89 September	53

16. SUPPLEMENTARY NOTATION

17. COSATI CODES		
FIELD	GROUP	SUB-GROUP

18. SUBJECT TERMS (Continue on reverse if necessary and identify by block number)
FEL, Free Electron Laser, Superconducting, Accelerator, GBFEL-TIE, Induction Linac, RF Linac, Misalignment, MO,MOPA, Amplifier, Self-Design, Wiggler, Tapered wiggler, Optical /Guiding

19. ABSTRACT (Continue on reverse if necessary and identify by block number)

This report describes the work performed by Science Applications International Corporation (SAIC) on the Strategic Defense Initiative Organization (SDIO) ground based laser (GBL) Systems Engineering and Technical Assistance (SETA) contract Task 3 - Laser Devices and Systems areas during 1989. An FEL amplifier code (FELAMP) has been developed under this contract and benchmarked with the FELEX code, developed by Los Alamos National Laboratory. The utility of the code is illustrated with different parameter sensitiviry analyses. Other SETA activities carried out under this contarct are also described.

20. DISTRIBUTION / AVAILABILITY OF ABSTRACT
☐ UNCLASSIFIED/UNLIMITED ☐ SAME AS RPT. ☐ DTIC USERS

21. ABSTRACT SECURITY CLASSIFICATION
unclassified

22a. NAME OF RESPONSIBLE INDIVIDUAL
Siva A. Mani

22b. TELEPHONE (Include Area Code)
(617) 863-5173

22c. OFFICE SYMBOL

D FORM 1473, 84 MAR 83 APR edition may be used until exhausted.

SECURITY CLASSIFICATION OF THIS PAGE

CONTRIBUTORS

Frederick G. Gebhardt
L. Scott Hills
Jerry E. Long
Siva Mani

ABSTRACT

This report describes the work performed by Science Applications International Corporation (SAIC) on the Stragetic Defense Initiative Organization (SDIO) ground based laser (GBL) Systems Engineering and Technical Assistance (SETA) contract Task 3 - Laser Devices and Systems areas during 1989. An FEL amplifier code (FELAMP) has been developed under this contract and benchmarked with the FELEX code, developed by Los Alamos National Laboratory. The utility of the code is illustrated with different parameter sensitivity analyses. Other SETA activities carried out under this contract are also described.

TABLE OF CONTENTS

		Page
	ABSTRACT	iii
	LIST OF FIGURES	v
	LIST OF TABLES	vii
1.0	SUMMARY	1
2.0	FEL AMPLIFIER MODELLING	3
	2.1 Introduction	3
	2.2 FEL Electron Dynamics and Photon Evolution	3
	2.3 Benchmarking the Code	6
	2.4 Results and Discussion	17
3.0	SSEB PARTICIPATION	26
4.0	SBFEL PROGRAM	27
	APPENDIX A -- Memorandum Written by Dave Quimby to Siva Mani on FELEX Code Runs for Comparison with FELAMP	39
	REFERENCES	53

LIST OF FIGURES

Figure		Page
1	Sensitivity of the FEL Efficiency to the Number of Calculational Steps	10
2	The Wiggler Taper as a Function of Distance as Calculated by FELEX Self-Design for the Parameters Listed in Table 1	11
3	Extraction Efficiency Versus Output Wavelength Using FELEX and FELAMP (SAIC) Codes	12
4	Extraction Efficiency Versus Brightness with FELAMP and FELEX Code Comparison	13
5	The Variation of Extraction Efficiency With Electron Beam Energy Spread. The Lines are Best Fit Curves Through the Calculated Points	14
6	Intensity of the Optical Field at Wiggler Entrance and at 20 m From the Entrance	15
7	Intensity of the Optical Field at the Center of the Wiggler and at the Exit Plane	16
8	Effect of Peak Current on the FEL Extraction Efficiency. If the Wiggler Taper Can Be Redesigned for Each Value of Current, One Can Obtain a Better Performance From the Wiggler	18
9	Effect of MO Power on FEL Efficiency. Redesign of the Taper For Lower MO Powers Provides For More Graceful Degradation of the FEL Performance	19
10	Effect of Energy Slew on the FEL Extraction Efficiency. With Lower MO Powers, the Effect is More Pronounced	21
11	Schematic of the Misalignment Problem Studied	22
12	Effect of Translational Misalignment on the FEL Performance. With Lower MO Powers, the Sensitivity of FEL Performance to Misalignment is Even Greater	23
13	FEL Performance for Exponentially Tapered Wigglers. The Self-Designed Wiggler Taper Gives an Extraction Efficiency of only About 12%	25
14	Schematic of TRW's Concept of Superconducting RFLFEL for a Space-Based Laser	28

LIST OF FIGURES (Continued)

Figure		Page
15	Principle of Harmonic Compensation Showing the Smaller Energy Spread and Longer Micro-Pulse Length Possible	30
16	TRW's Scheme for Careful Phase Space Control and Near Perfect Energy Recovery	32
17	Technical Approach by PI for HCRF Accelerator	33
18	Schematic of the HCRF Accelerator by PI	34
19	The HCRF Pulse Format as Proposed by PI. The FEL Macropulse Length Would be Shorter by the Filling Time	36
20	HCRF Component Efficiency Goals for SBFEL	37

LIST OF TABLES

Table		Page
1	FEL Amplifier Parameters for Test Run	8
2	Effect of Random Number Seed on the FEL Efficiency. Increasing the Number of Particles Decreases the Differences	9
3	Requirements for the HCRF SBFEL System as Envisioned by PI .	38

1.0 SUMMARY

Directed Energy (DE) technologies such as high power lasers and neutral particle beams are considered to offer great potential for the strategic applications of Ballistic Missile Defense. Both the Army and the Air Force are actively engaged in extensive DE research and technology development programs for the Ground Based Lasers (GBL) sponsored by the SDI for the BMD. The Army, through the USASDC, is managing the Ground Based Free Electron Laser (GBFEL) program funded by the SDIO. The primary emphasis of the Army FEL program is the GBFEL Technology Integration Experiment (GBFEL-TIE) at the White Sands Missile Range to demonstrate the integration of a high power laser system with a large beam control system and the propagation of the high power laser beam with phase compensation through the turbulent and blooming atmosphere with adequate beam quality at the top of the atmosphere. The two candidate laser systems under consideration by the Army for the GBFEL-TIE are the RF Linac FEL and the Induction Linac FEL. These two technologies are vigorously pursued by teams led by Boeing and TRW respectively. The Army is presently competing these two laser systems for down selection into one system that will get built at the WSMR facility. Much of our effort during the past year has been spent on reviewing the efforts that are undergoing at Boeing and Lawrence Livermore National Laboratory (TRW's team member), assisting in the Source Selection Assessment, developing computational tools to help in the Source Selection Assessment and in reviewing other FEL programs, notably the Space-based FEL programs, that are funded by SDIO through its agents.

In the next section, we describe the results of the modelling of the FEL amplifier. This model treats the motion of the individual electrons that are distributed in the six-dimensional phase space as they travel through the tapered wiggler. The betatron motion of the electrons in the xz and yz plane is included. The evolution of the optical field is treated by solving the paraxial wave equation. Our program also calculates the energy balance between the optical field and the electron energy independently and ensures that this is maintained within acceptable tolerance. Our numerical model was benchmarked to the FELEX code developed at the Los Alamos National Laboratory. The code has then been used to study the effect of peak current, brightness, MO power etc. on the extraction efficiency. We have also used the code to

verify the design of the wiggler and other FEL parameters proposed by the two competing teams. The results of these calculations were used in the Source Selection assessment. Our efforts in the participation of the Source Selection Evaluation Board (SSEB) are briefly summarized in Section 3.

SDIO has been pursuing the development of alternate FEL technology for the space-based FELs. The primary emphases in this area have been in the development of superconducting and cryogenic accelerator technologies at TRW and LANL respectively. Other areas include the development of the relativistic klystron and aerolenses for shortening the optical cavity lengths. These are discussed in Section 4.

2.0 FEL AMPLIFIER MODELLING

2.1. INTRODUCTION

In our previous work[1], we had modelled the FEL gain interaction inside a wiggler amplifier using the resonant particle approximation. In that model, a complex two-dimensional field (in x and y) is propagated through the wiggler along the z-direction. For each grid point in x and y, we tracked one electron assumed to be resonant in the ponderomotive potential well. To account for the fact that only some electrons are trapped in the ponderomotive potential well and only these electrons contribute to the gain of the free electron laser, we calculated a quantity called the trapped fraction based on the ponderomotive potential well depth and the energy spread of the electron beam. While this is not entirely satisfactory, this method yielded reasonable results. For very long amplifiers with high gain, this model was good only in predicting qualitative behavior with respect to parameter variations. Furthermore, the model does not take into account the details of particle distribution in the 4-dimensional transverse phase space, nor does it take into account the betatron motion of the electrons in the wiggler. For these reasons we decided to develop a full 3-dimensional model of the FEL interaction in a wiggler amplifier. This model tracks individual electrons and is the equivalent of the FRED code developed by Ted Scharlemann of LLNL and FELEX code developed by Brian McVey of LANL. FELEX is a more general code than FRED and can treat multiple frequencies that are present due to the existence of sidebands. The code that we have developed is similar to FRED in that it treats a single optical frequency but is fully 3-dimensional like FELEX in all other aspects. The FELEX code has been benchmarked with FRED and our code has been benchmarked with FELEX. In the next section, we describe the salient features of our code and the method of solution. In Section 2.3, we describe the results of benchmarking our code with FELEX.

2.2. FEL ELECTRON DYNAMICS AND PHOTON EVOLUTION

The equations that describe the dynamics of the electrons and the evolution of the optical flux inside a wiggler have been discussed by Scharlemann[2], Tokar et al.[3], Colson and Ride[4], and others previously. The

wave equation is usually simplified using the slowly-varying amplitude and phase approximation to obtain the paraxial equation with a driving term that describes the coupling between the light and the electrons. In addition, the electron equations are simplified by averaging over a wiggler period. For simplicity, we shall assume that we have a linearly polarized wiggler with equal plane curved-pole focussing geometry. The code that we have developed can treat helical wigglers as well as planar wigglers. The equations of motion of the electrons are somewhat simplified with equal plane curved pole focussing feature. Following Scharlemann's notation, the paraxial wave equation with the source term describing FEL interaction is

$$\frac{\partial E_s}{\partial z} = \frac{i}{2k} \nabla_\perp^2 E_s + \tfrac{1}{2} Z_0 a_w f_B J \left\langle \frac{e^{-i\theta_j}}{\gamma_j} \right\rangle, \qquad (2.1)$$

where E_s is the complex amplitude of the electric field of the wave, a_w is the normalized, dimensionless, r.m.s. vector potential of the wiggler, Z_0 is the impedance of free space, $J(x,y,z)$ is the current density, and f_B is the coupling coefficient which depends on the wiggler geometry. The value of f_B is equal to 1 for helical polarization, and equal to $J_0(\mu) - J_1(\mu)$ for linear polarization where $\mu = a_w^2 /2(1 + a_w^2)$. The angle brackets in Eq. (1) denote an average over N electrons in one optical wavelength, and

$$\theta_j = (k_s + k_w)z_j - \omega t, \qquad [j = 1, \ldots, N] \qquad (2.2)$$

is the longitudinal position of an electron with respect to the ponderomotive potential formed by the wiggle motion and the plane electromagnetic wave propagating at c. Here k_s and k_w are the optical and wiggler wavenumbers respectively and ω is the frequency of light. If ϕ is the phase of the electric field, the phase of an electron in the actual ponderomotive potential well is given by

$$\psi_j = \theta_j + \phi. \tag{2.3}$$

The differential equations that describe the electron dynamics are given by

$$\frac{d\gamma_j}{dz} = -\frac{a_w f_B e_s}{\gamma_j} \sin \psi_j, \tag{2.4}$$

$$\frac{d\theta_j}{dz} = k_w - \frac{k_s}{2\gamma_j^2}\left(1 + a_w^2 - 2a_w a_s \cos\psi_j + \gamma^2\beta_{\perp j}^2\right), \tag{2.5}$$

where $e_s = eE_s/mc^2$ and $a_s = e_s/k_s$.

In FELAMP, the paraxial wave equation is solved by symmetric split operator technique, while the electron equations are solved by fourth-order Gill method which is a form of Runge-Kutta solver. In the split operator technique, the paraxial wave equation is first solved without the source term on the right hand side of Eq. (2.1) for a distance $\Delta z/2$. We then suppress the transverse gradient terms in Eq. (2.1) and solve for the evolution of the field due to the source term over a distance Δz. This is carried out using Gill's method with an ordinary differential equation solver, while at the same time solving Eqs. (2.4) and (2.5). Finally we apply the homogeneous paraxial wave equation solution over a distance $\Delta z/2$ to complete the evolution of the field over a total distance Δz. If the step size z is reasonably small, this technique would provide a stable solution to the problem. We assume equal plane focussing in both xz and yz planes and write an analytical expression for the betatron motion of the electrons as follows:

$$x_\beta = \frac{x_{\beta 0}}{\sqrt{k_{\beta x}}} \cos\left(\int k_{\beta x}\, dz + \varphi_x\right), \tag{2.6}$$

$$y_\beta = \frac{y_{\beta 0}}{\sqrt{k_{\beta y}}} \cos \left(\int k_{\beta y}\, dz + \varphi_y \right) \qquad (2.7)$$

where $k_{\beta x} = k_{\beta y} = k_w a_w/\sqrt{2}\ \gamma$ are the x and y betatron wavenumbers respectively. $x_{\beta 0}$ and $y_{\beta o}$ are the initial betatron amplitudes while φ_x and φ_y are the initial betatron phases. Equations (2.6) and (2.7) represent the WKB approximation to the zeroth order motion of the electrons through the wiggler due to betatron motion. These solutions are valid for parabolically curved pole focussing which provide equal plane focussing. For a more general focussing scheme, such as the canted pole focussing, the solutions for the betatron motion may be obtained by solving simple differential equations. The homogeneous paraxial wave equation is readily solved using FFT techniques on a 128 x 128 or 256 x 256 transverse grid. To obtain reasonable accuracy for a long wiggler, the number of Δz steps required are at least 200. The number of electrons needed to achieve adequate accuracy is in the 4000 to 8000 range.

It is interesting to note that neither FRED nor FELEX uses FFT algorithms for the free space propagation. FELEX uses a finite difference ADI algorithm to solve the paraxial wave equation in three dimensions with the source function in Eq. (2.1) being estimated forward in time using an Adams-Bashforth predictor formula. FRED, on the other hand, assumes cylindrical symmetry for the field and solves it in two dimensions (r and z) using a finite element method, which permits a unique weighting of particles to radial grid points. In as much as the present method and FELEX treat the paraxial wave equation in three dimensions fully, these two are readily comparable while some differences may exist between the results of FRED and our present method.

2.3. BENCHMARKING THE CODE

A number of checks were initially carried out to test the stability of the numerical scheme. The code runs on any 80386 microcomputer with extended memory and math co-processor using A.I. Architects' OSx86 operating system and Lahey compiler. For 100 steps on a 128 x 128 grid it takes approximately 40

minutes for the code to run. Table 1 gives a list of the parameters that were used for the initial runs. The electrons' initial distribution is generated using a random number generator. We were surprised to see a wide variation in our results depending on the seed value used in the random number generator, but later found out that other codes give similar variation. The extraction efficiency varied as much as 25% in some cases. The variation was of course greater with smaller number of total particles tracked through the wiggler. Most of the runs were carried out with 4096 particles to compare with runs from the FELEX code. Figure 1 shows the effect of varying the calculational step size on the extraction efficiency. From the figure we see that good convergence of the results is obtained with as few as 200 steps. Table 2 shows the variation in the extraction efficiency with different random number seed values. Similar variation is said to be exhibited by the FRED code.

To benchmark our code, we asked Dave Quimby of STI to run the FELEX code for the list of input parameters provided in Table 1. The FELEX self-design feature was invoked and its taper prescription was provided to us. This taper is plotted in Fig. 2 showing a_w as a function of z. Using the same taper, we ran our code and compared our results with FELEX code. A number of runs were performed on the FELEX so that our code could be benchmarked extensively. A memo written by Quimby on the results of the FELEX runs is attached as an Appendix to this report. Figure 3 shows the extraction efficiency as a function of input wavelength using both the FELEX and the SAIC codes. Since the two codes use different random number generators and different starting seed values, we cannot expect agreement better than a few percent. The agreement is rather good over the entire range of wavelengths scanned. Figure 4 shows the comparison between the two codes as a function of electron beam brightness. Once again the agreement is good. We then varied the energy spread of the electron beam and our results are plotted in Fig. 5. The agreement at low extraction efficiencies is usually not good because it is a sensitive function of the initial phase space distribution of the electrons. For different seed values, a much wider variation in the answers is seen at low extraction efficiencies than at high extraction efficiencies. Finally, in Figs. 6 and 7, we show the intensity and phase profiles at different stations inside the wiggler for the nominal case.

Table 1

FEL AMPLIFIER PARAMETERS FOR TEST RUN

E-BEAM

γ = 392.4 (E = 200 MeV)

I = 2000 A

$\Delta\gamma/\gamma$ = 0.1 % (Gaussian, Full Width at 1/e Points)

Normalized Edge Emit = 447 π mm-mrad

Brightness = (2I)/(emit**2) = 2.E5 A/(cm-rad)**2

Edge Radius = 0.22 cm

Uniformly-Filled 4-Space

4096 electrons

WIGGLER

L_w = 100 m

B = 3.19 kG (a_w = 1.688)

Period = 8.0 cm

Curved-Pole Focus

Self Designed Taper for

Constant ψ_R = 20 degrees at Radius = 0.65 R_{eb}

OPTICAL BEAM

λ = 1.0 micron

Input Power = 100 MW

Rayleigh Range = 48 m

Beam waist at wiggler entrance

Waist Radius = 0.39 cm (1/e**2 intensity)

GRID

128x128 cells out to (x,y) = 1.65 cm

Axial step size = 12.5 cm

Table 2

Effect of Random Number Seed on the FEL Efficiency. Increasing the number of particles Decreases the Differences

Brightness $(amp/cm\text{-}rad)^2$	Extraction Efficiency, %				
	FELEX	SAIC 1	SAIC 2	SAIC 3	SAIC 4
1×10^5	9.1	8.24	14.68	10.22	16.53
2×10^5	24.0	25.26	24.66	26.11	25.27
4×10^5	30.0	29.76	27.88	30.80	27.81

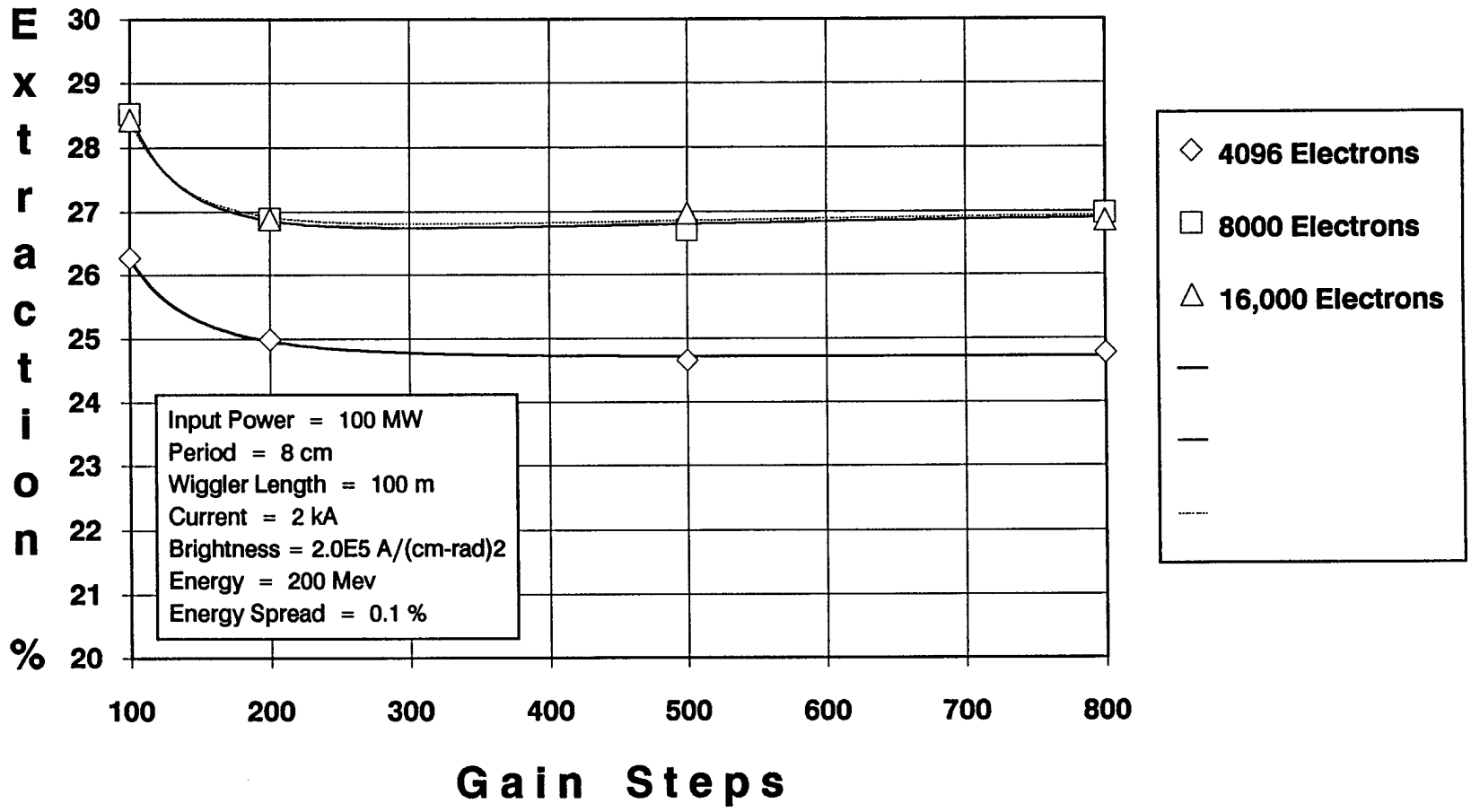

FIG. 1. SENSITIVITY OF THE FEL EFFICIENCY TO THE NUMBER OF CALCULATIONAL STEPS.

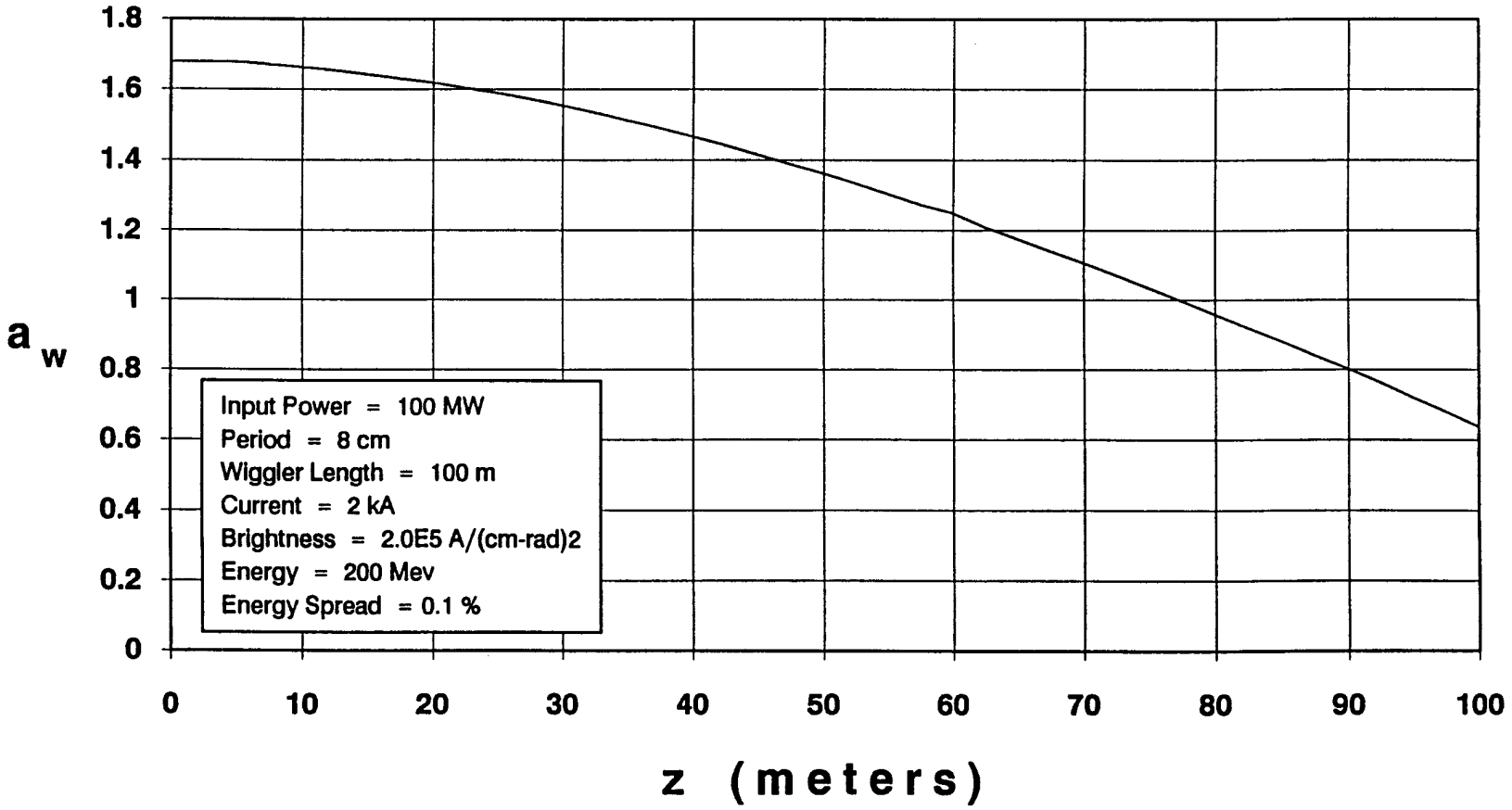

FIG. 2. THE WIGGLER TAPER AS A FUNCTION OF DISTANCE AS CALCULATED BY FELEX SELF-DESIGN FOR THE PARAMETERS LISTED IN TABLE 1.

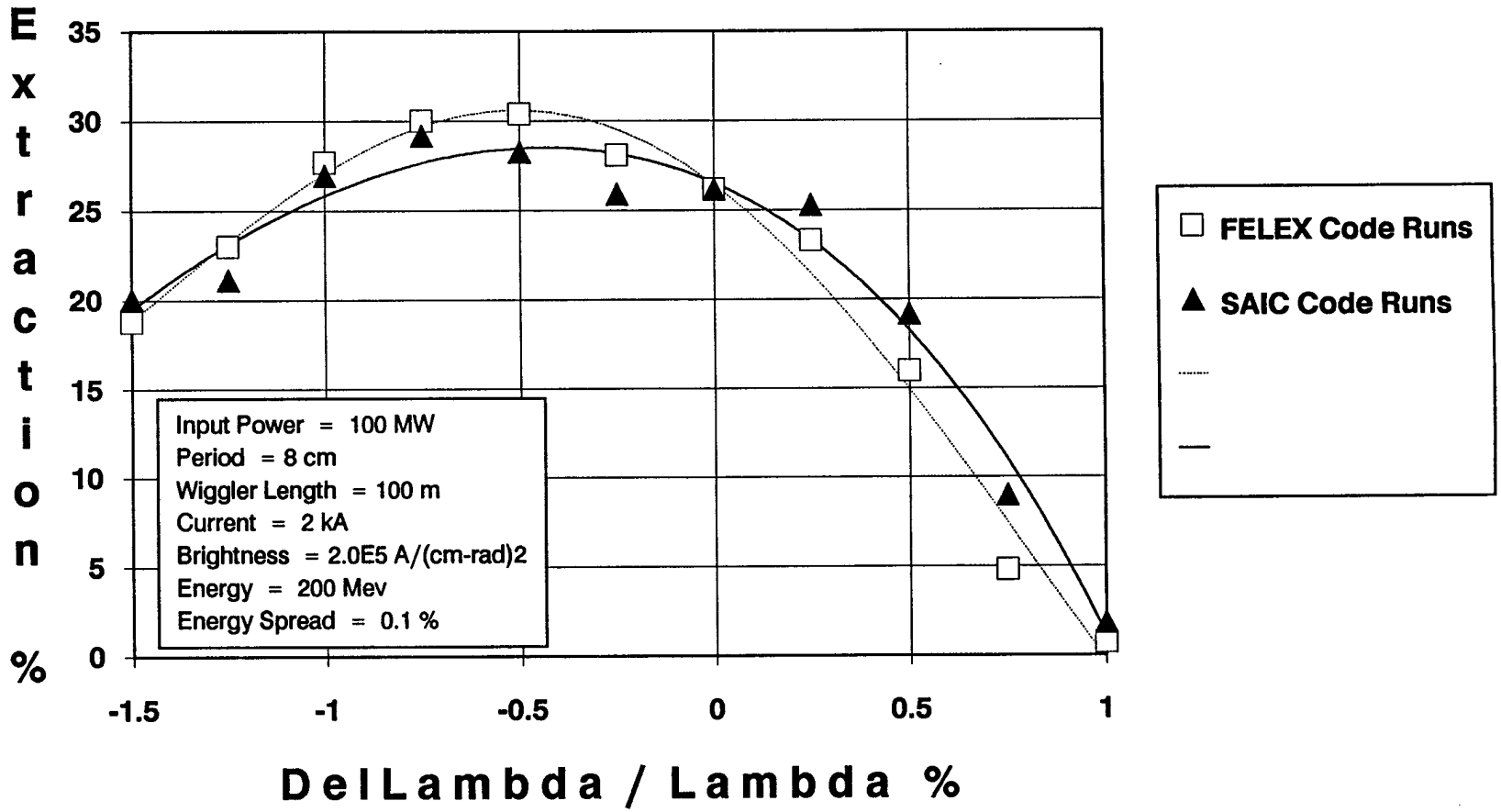

FIG. 3. EXTRACTION EFFICIENCY vs OUTPUT WAVELENGTH USING FELEX AND FELAMP (SAIC) CODES.

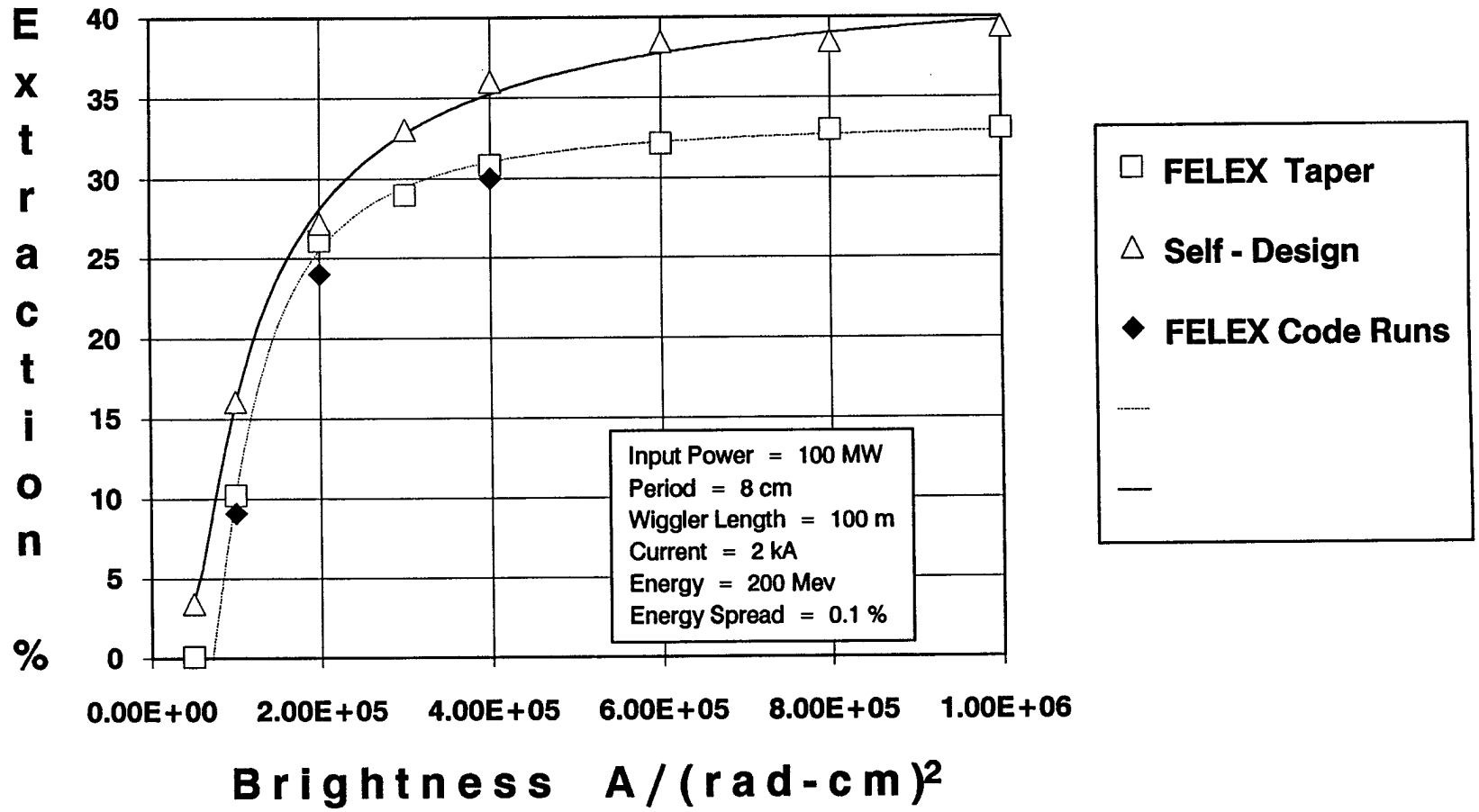

FIG. 4. EXTRACTION EFFICIENCY VS BRIGHTNESS WITH FELAMP & FELEX CODE COMPARISON.

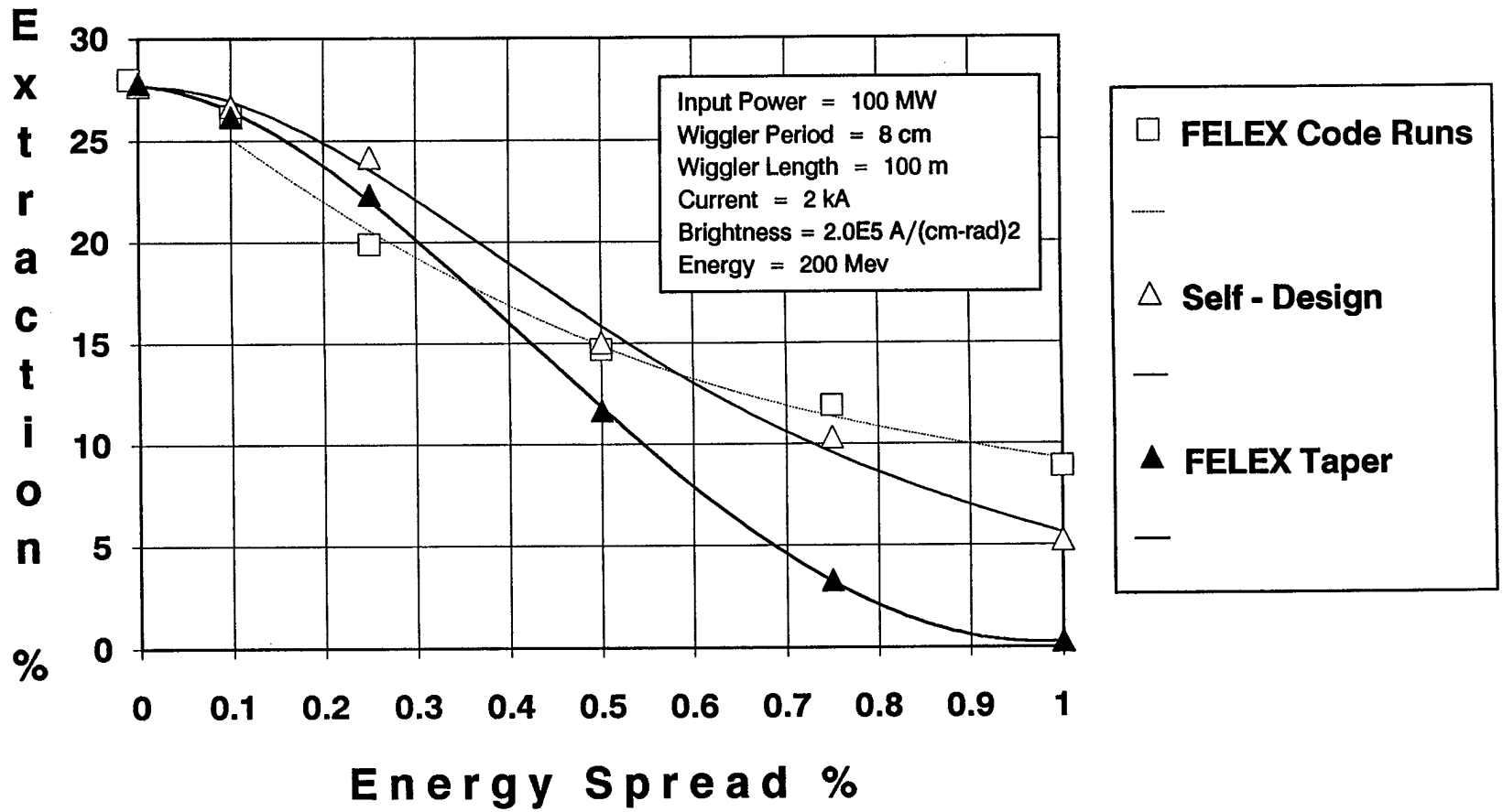

FIG. 5. THE VARIATION OF EXTRACTION EFFICIENCY WITH ELECTRON BEAM ENERGY SPREAD. THE LINES ARE BEST FIT CURVES THROUGH THE CALCULATED POINTS.

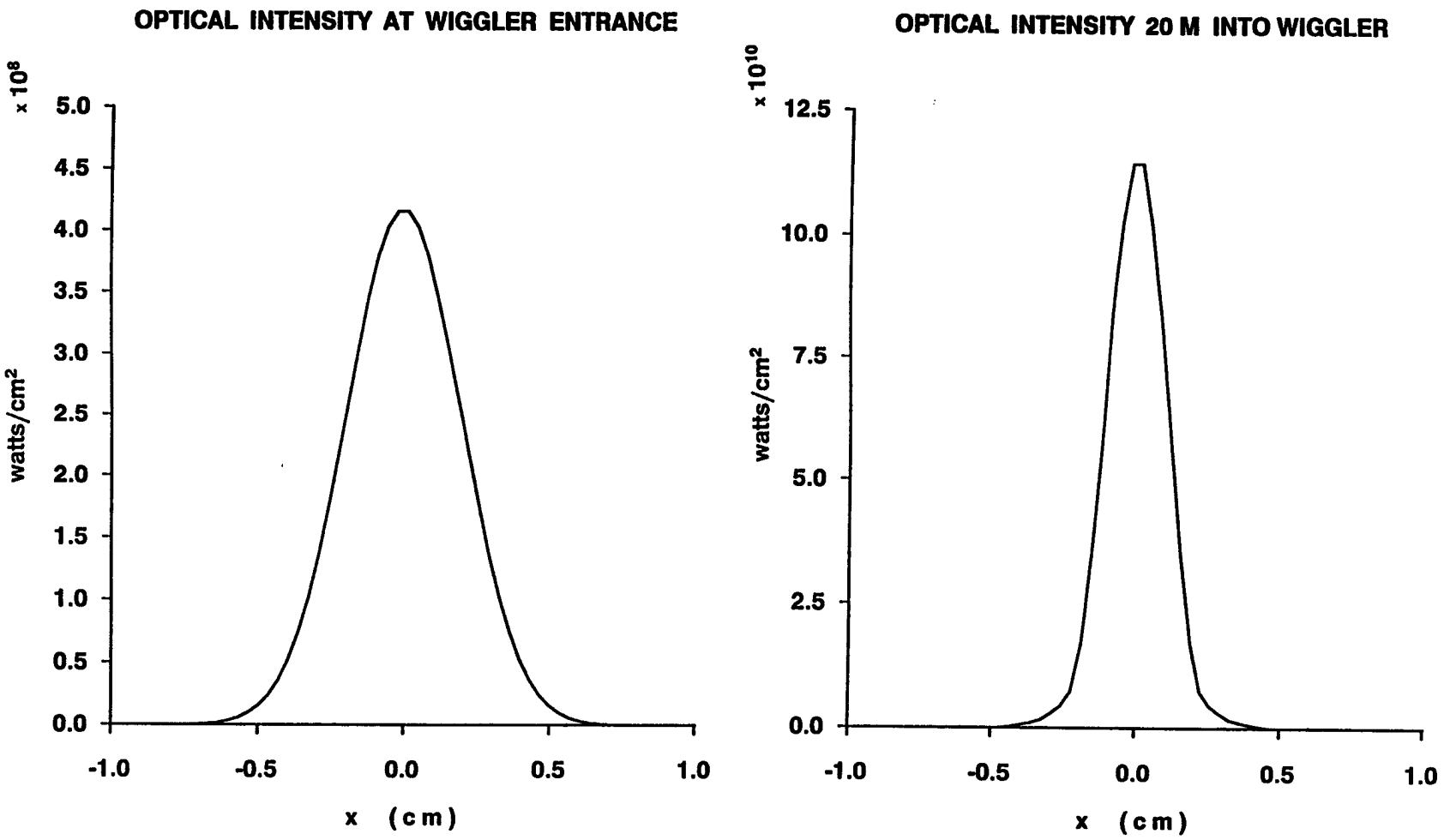

FIG. 6. INTENSITY OF THE OPTICAL FIELD AT WIGGLER ENTRANCE AND AT 20 m FROM THE ENTRANCE.

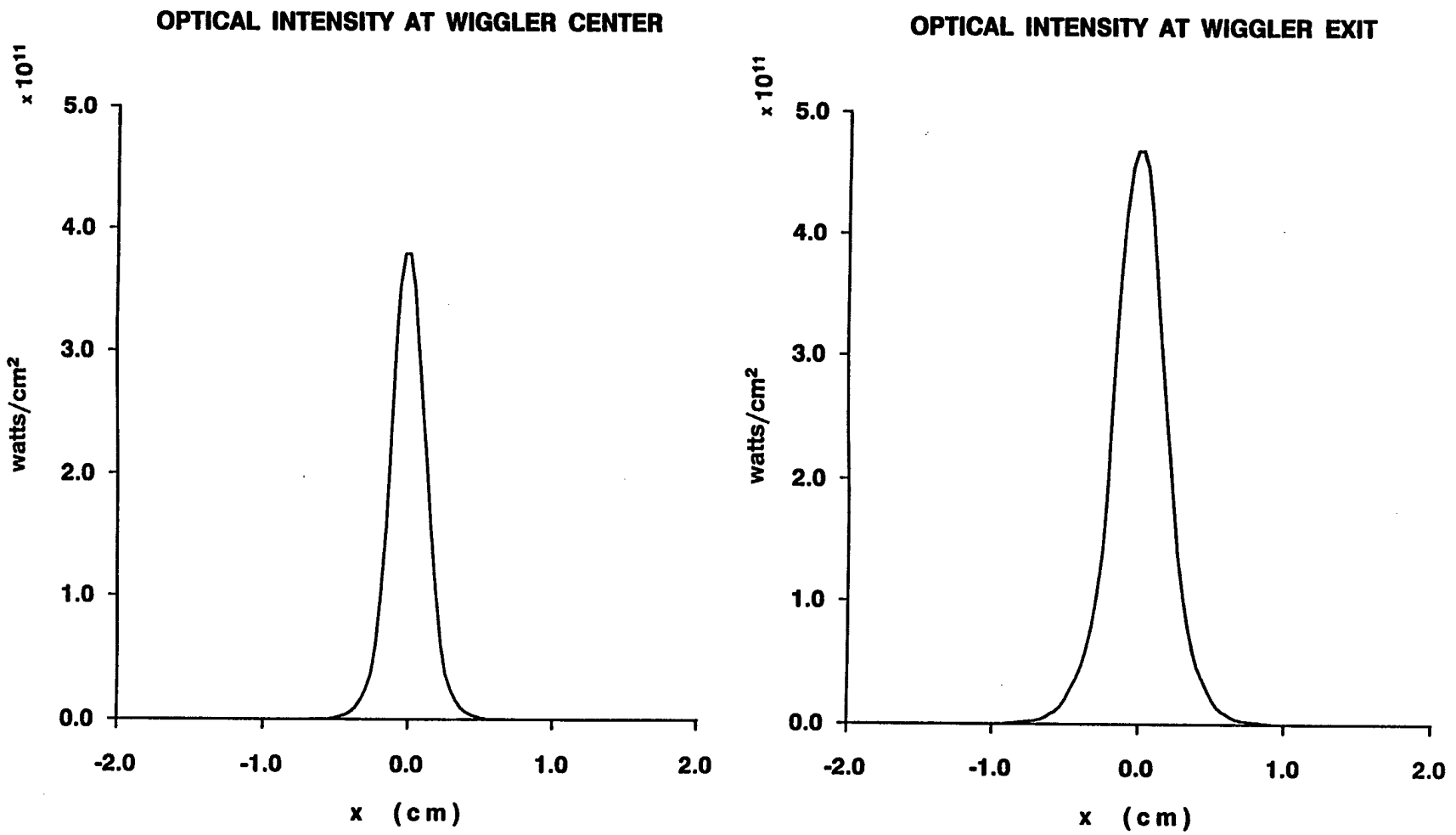

FIG. 7. INTENSITY OF THE OPTICAL FIELD AT THE CENTER OF THE WIGGLER AND AT THE EXIT PLANE.

2.4 RESULTS AND DISCUSSION

Having benchmarked the FELAMP code with FELEX, it was exercised to study the effect of different FEL parameters on the extraction efficiency. The four important parameters in the FEL amplifier are the peak current, MO power, Energy slew and Wiggler misalignment. For the benchmark case, Fig. 8 shows the effect of peak current on efficiency. As expected, extraction efficiency increases with the peak current. Two curves are shown in Fig. 8. In the first curve, the taper prescription is kept fixed as the current is changed. This corresponds to possible current variations within a single pulse or in a time scale small compared to the time it takes to change the wiggler field. In the second curve, the wiggler is self-designed at each current. This is what one might do if one knows a priori that the peak current from the accelerator has gone up or down. The current droop necessary in an induction FEL to keep the beam energy reasonably constant is ~ ± 5%. Averaged over the pulse length, the effect of this variation on the average power is negligible to first order.

Figure 9 shows the effect of MO power on the extraction efficiency. For a fixed wiggler taper, the extraction efficiency steadily drops as the MO power is reduced over 2 orders of magnitude. If one redesigns the wiggler at each input power level, we see that the degradation of the FEL performance is more graceful. What one really wants to find out is whether this curve has a 'knee' as one lowers the MO power. If there is a MO power level below which the extraction efficiency drops nonlinearly and precipitously, one should design the FEL amplifier with the MO power chosen to be at least an order of magnitude above this critical power.

In the induction linac, the saturation of the ferrite core makes the impedance a nonlinear function of the B-field and therefore becomes time-dependent during the pulse. This results in a voltage droop across the gap during a single pulse. Since the wavelength of the MO is fixed and the wiggler parameters cannot be changed during the pulse, one encounters unacceptable performance degradation if the energy droops too much. To compensate for this droop, it has been proposed to decrease the current during the pulse. In spite of this decreased load, it is anticipated that the energy of the

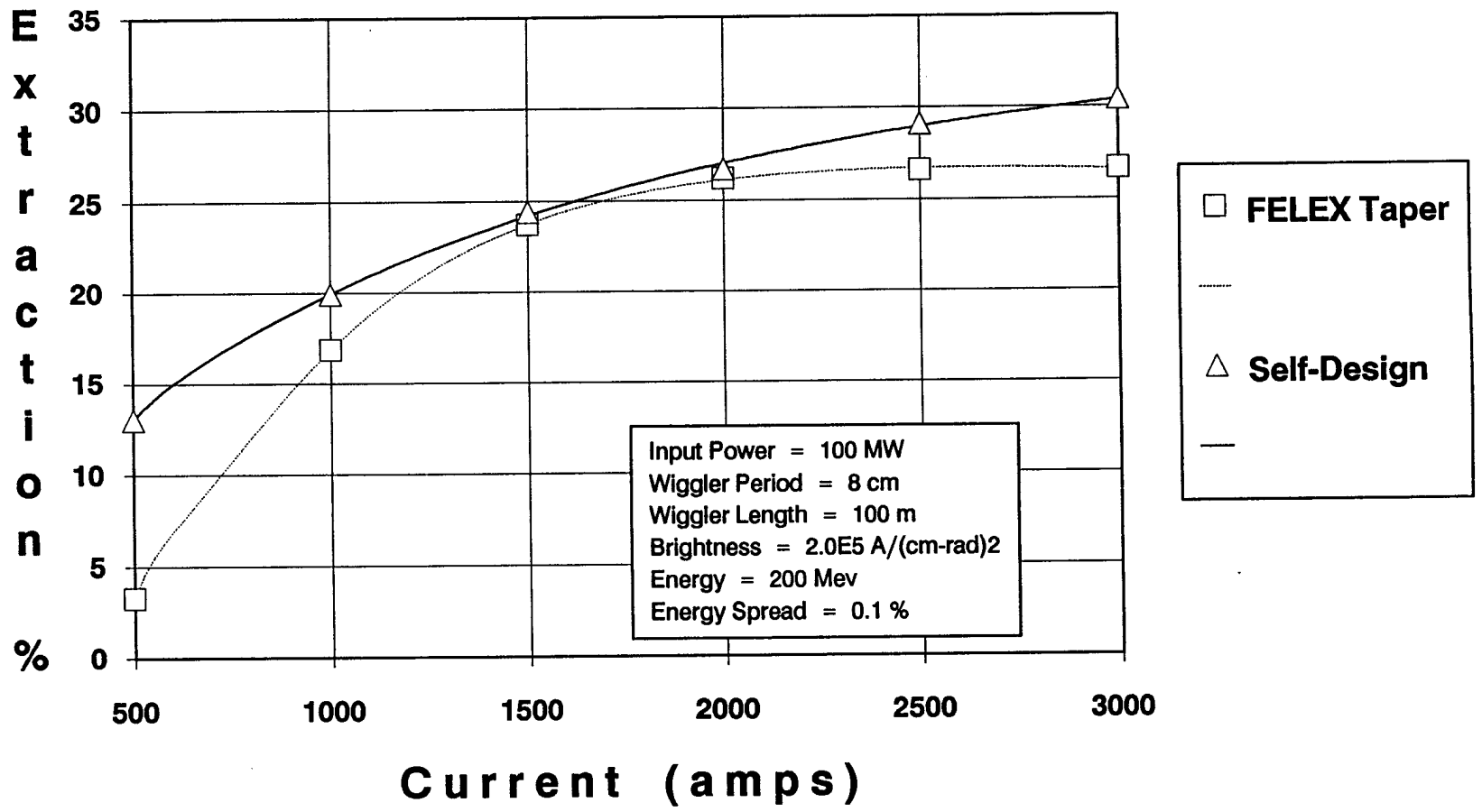

FIG. 8. EFFECT OF PEAK CURRENT ON THE FEL EXTRACTION EFFICIENCY. IF THE WIGGLER TAPER CAN BE REDESIGNED FOR EACH VALUE OF CURRENT, ONE CAN OBTAIN A BETTER PERFORMANCE FROM THE WIGGLER.

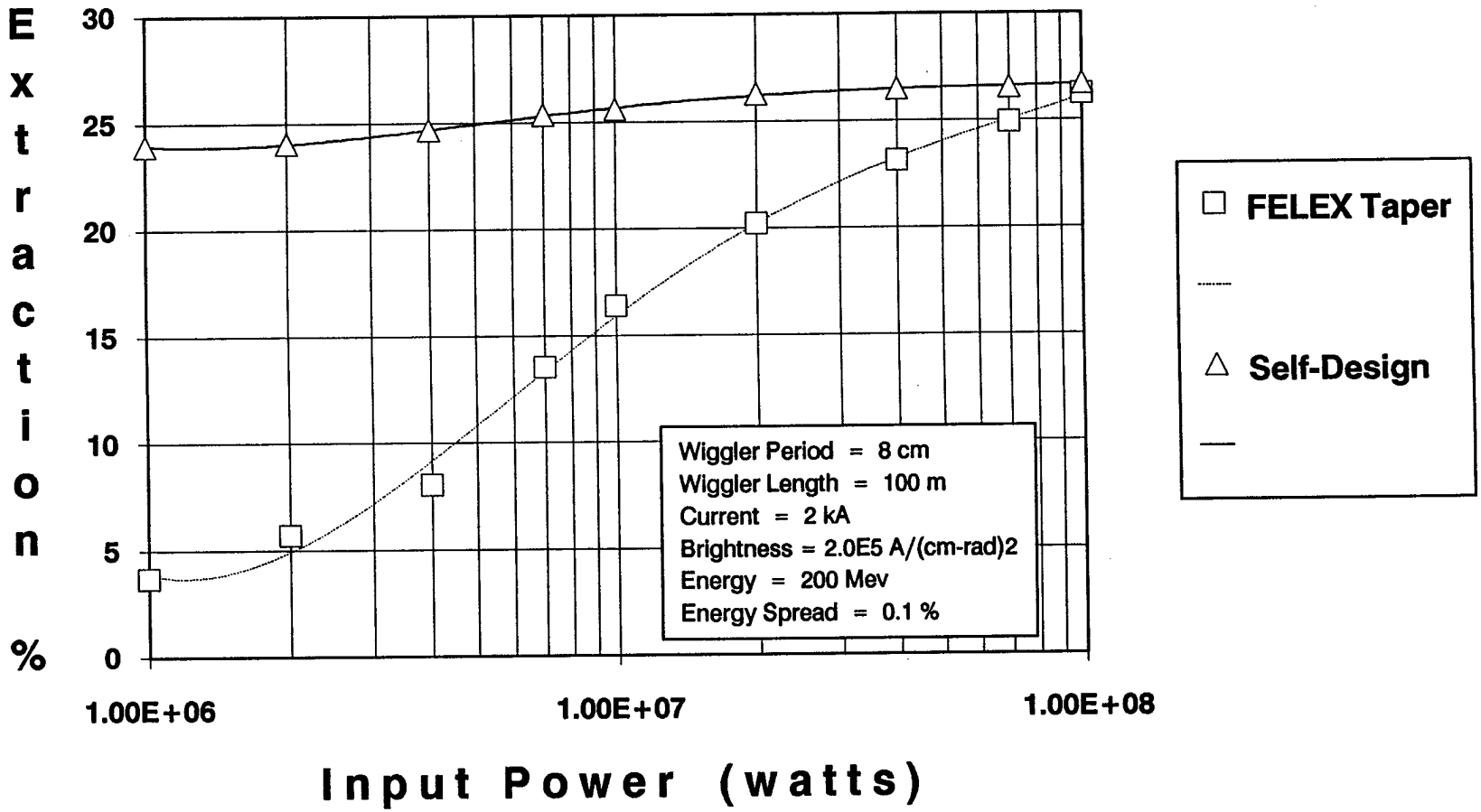

FIG. 9. EFFECT OF MO POWER ON FEL EFFICIENCY. REDESIGN OF THE TAPER FOR LOWER MO POWERS PROVIDES FOR MORE GRACEFUL DEGRADATION OF THE FEL PERFORMANCE.

electron beam will vary by as much as ± 0.4% during the pulse. Figure 10 shows the effect of energy slew on the extraction efficiency. Typically, averaged over the pulse length of an induction linac pulse, an energy slew of ± 0.4% leads to an efficiency degradation of 20 to 30%. This shows the importance of keeping the energy slew to an absolute minimum.

One of the common problems with very long wigglers is their alignment. The wiggler is typically fabricated in sections of 4 to 5 meters long. When the individual sections are assembled, not only should the geometric axis of the individual sections align with respect to a nominal axis, but their magnetic axes should also be aligned. Any misalignment in the wiggler axis, translational or angular, would cause degradation in the FEL performance. The FELAMP code has been written to take into account possible wiggler misalignments in order to investigate their effect on the amplifier performance. The code can take into account the translational misalignment of the sections of the wiggler or sinusoidal or random tilt of the sections of the wiggler. A schematic of the translational misalignment is shown in Fig. 11. In the program, we specify the maximum off-set that a section of the wiggler can have with respect to the nominal axis and assign at random an off-set within these bounds for each section. Figure 12 shows the effect of misalignment on the extraction efficiency for the parameters shown in Table 1. Studies of this type enable one to specify the manufacturing and fabricating tolerance on the wiggler assembly. Typical tolerance requirements for a 100 meter long wiggler are that the off-set be no more than 100 μm and the angular misalignment be no more that 1 μrad.

The self-design feature of the wiggler allows one to design the wiggler without any a priori knowledge of the best taper. In the self-design, a single design electron is kept at some design phase angle. Since it is possible to change the design phase angle as a function of the distance in to the wiggler, it is not clear which design will give the best FEL performance. In our earlier one-dimensional analysis,[6] we have found that an exponential taper of the following form for the wiggler vector potential gives the best performance:

$$a_w = a_{w0} \exp \{- \alpha (z/L_w)^n\} \qquad (2.8)$$

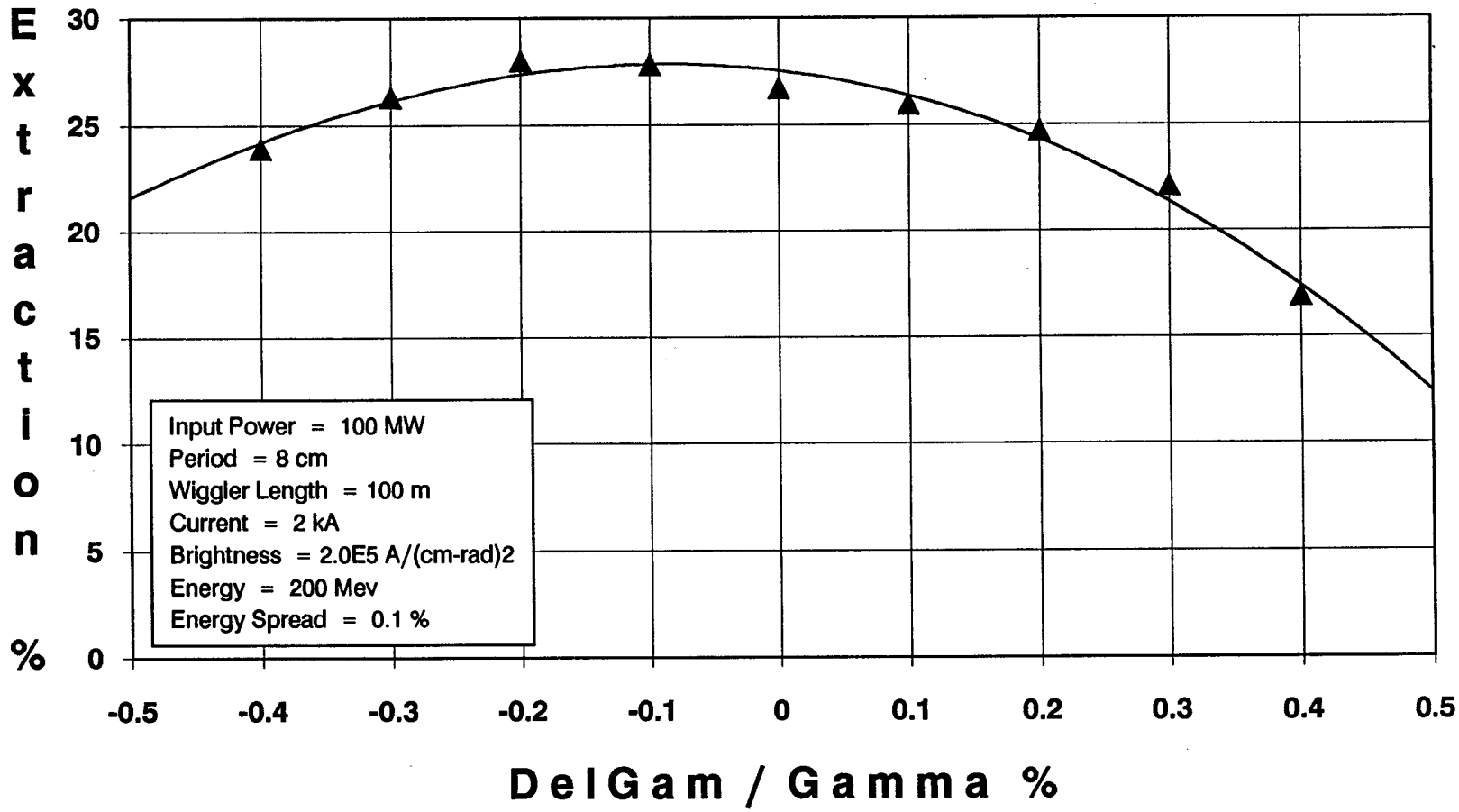

FIG. 10. EFFECT OF ENERGY SLEW ON THE FEL EXTRACTION EFFICIENCY. WITH LOWER MO POWERS, THE EFFECT IS MORE PRONOUNCED.

- EACH WIGGLER SECTION IS OFF-SET BY A RANDOM AMOUNT FROM THE DESIRED AXIS

- WIGGLER SECTION LENGTH AND MAXIMUM RANDOM OFF-SET ARE VARIABLE PARAMETERS

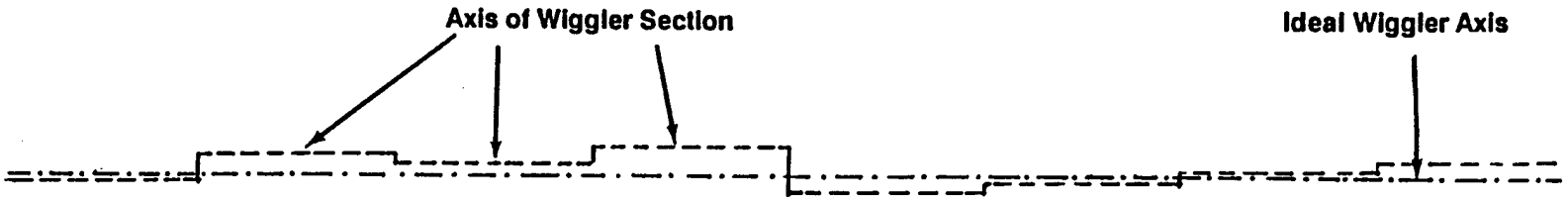

FIG. 11. SCHEMATIC OF THE MISALIGNMENT PROBLEM STUDIED.

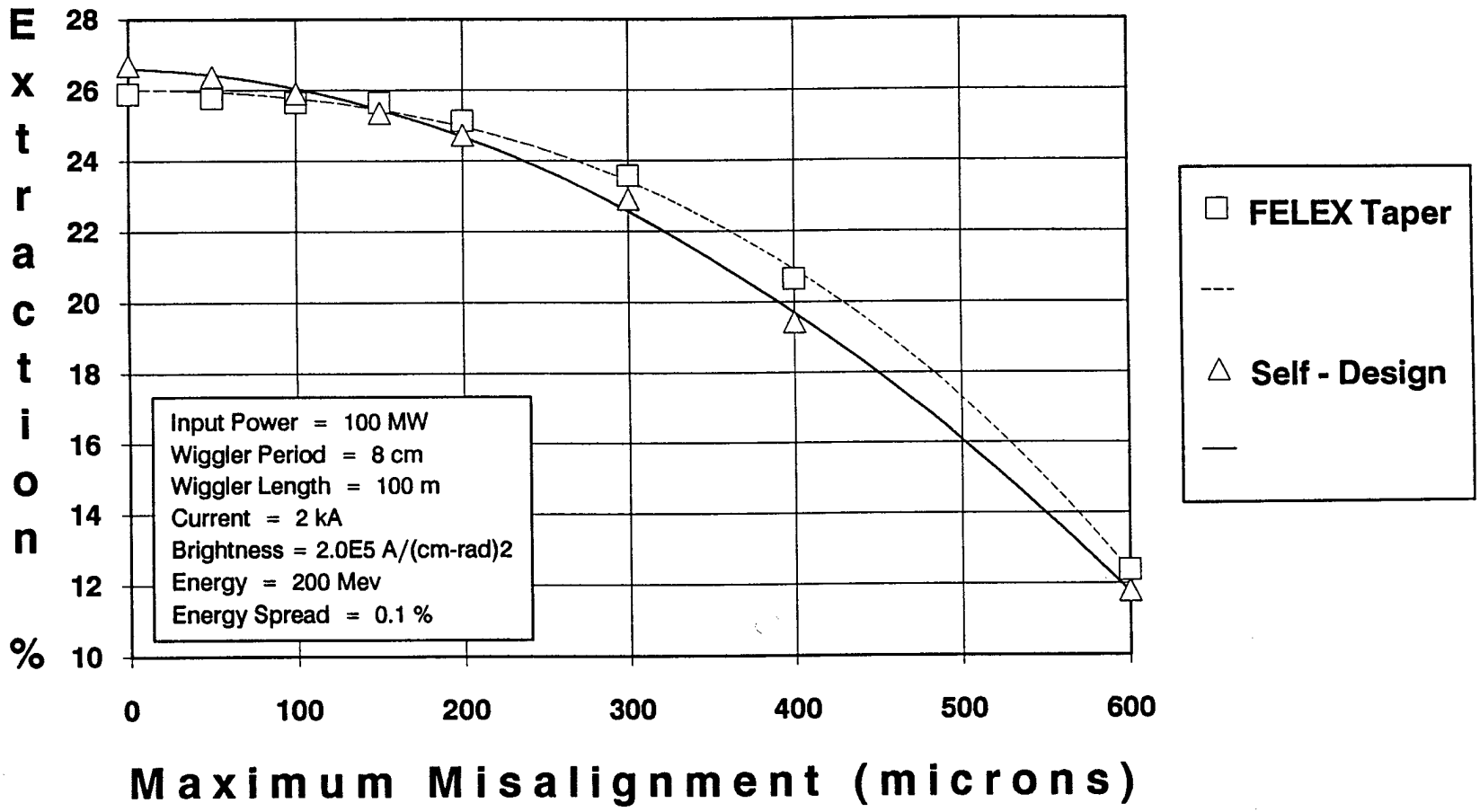

FIG. 12. EFFECT OF TRANSLATIONAL MISALIGNMENT ON THE FEL PERFORMANCE. WITH LOWER MO POWERS, THE SENSITIVITY OF FEL PERFORMANCE TO MISALIGNMENT IS EVEN GREATER.

where a_{w0} is the initial value for the wiggler vector potential, L_w is the length of the wiggler and α and n are constants. Figure 13 shows the extraction efficiency as a function of the exponent n for different values of α for a typical set of optical and electron beam input parameters. The best efficiency that can be obtained is >15% for an exponent of ≈3.5. In comparison to this, the self-design feature gives an extraction efficiency of ≈12%. A substantial improvement in the extraction efficiency can be obtained using the exponential taper. The strategy for designing the wiggler would be as follows: First, we design the wiggler with the self-design feature and obtain the initial value of a_{w0}. Knowing the final value of a_w, we can calculate α. One can then try different values of n to maximize the efficiency. The value of α can also be varied around the first calculated value to find the design that gives the best FEL performance.

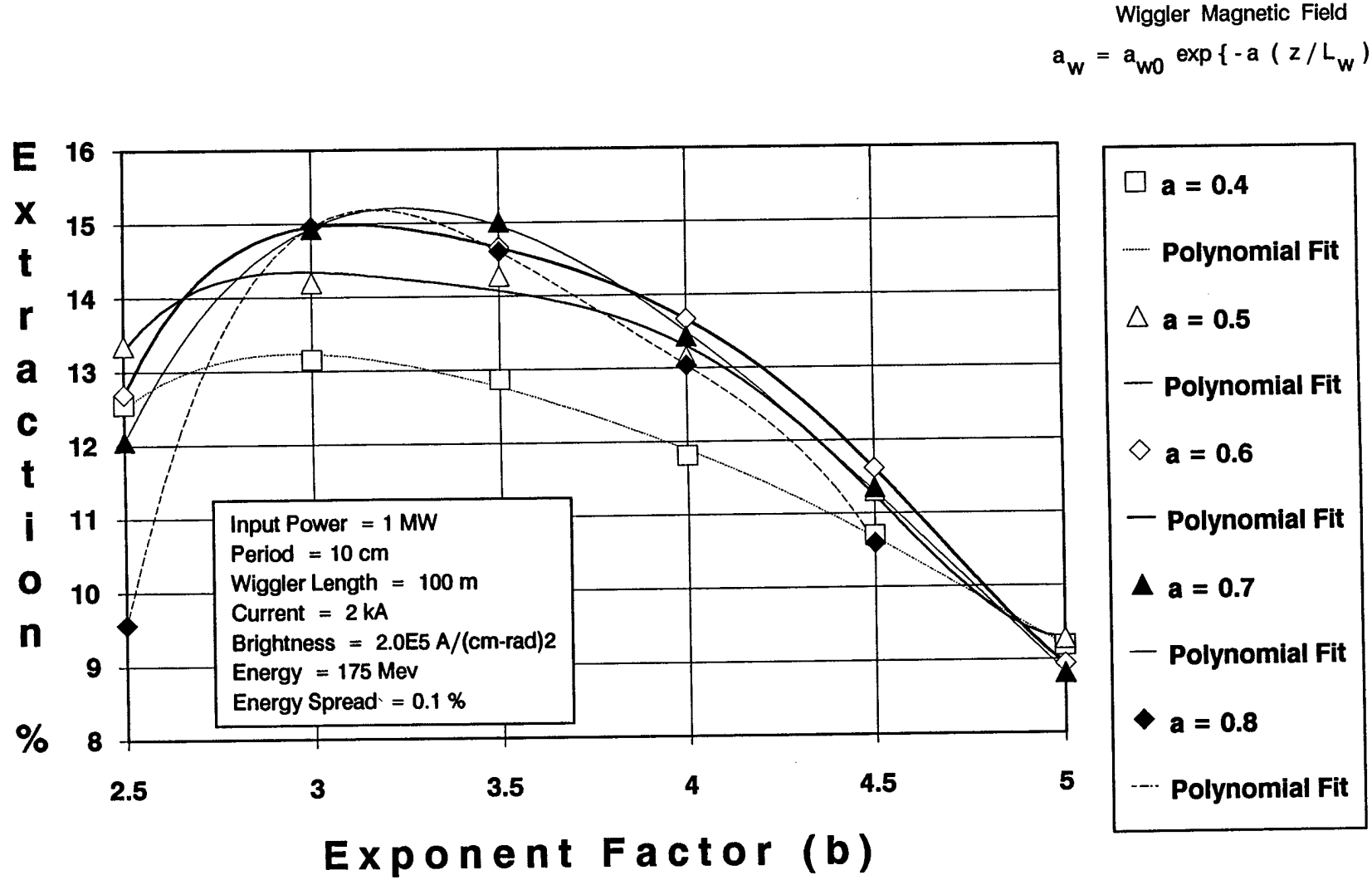

FIG. 13. FEL PERFORMANCE FOR EXPONENTIALLY TAPERED WIGGLERS. THE SELF-DESIGNED WIGGLER TAPER GIVES AN EXTRACTION EFFICIENCY OF ONLY ABOUT 12%.

3.0 SSEB PARTICIPATION

The U.S. Army SDC initially competed the two leading FEL technologies for constructing a laser sub-system for the GBFEL-TIE at a power level of Q (classified value). The team led by Boeing Company submitted a proposal to build a RF Linac FEL to deliver the required power at the stated wavelength to the beam control system. The team led by TRW submitted a proposal to build an induction linac FEL with the same overall requirements. As part of the 'Outside Resources,' Siva Mani from SAIC participated in the assessment of the two proposals and assisted the Source Selection Evaluation Board (SSEB). To facilitate the assessment, the FEL amplifier code was exercised to verify the design of the two teams. The assessment was conveyed to the USASDC orally and in written form. Since the Army has not completed its selection of the LSS contractor, the results of our findings will not be reported here.

Since the initial request for proposal by the Army, SDIO has found it necessary to descope the GBFEL-TIE system due to budgetary constraints. Accordingly, in May of this year a revised RFP was issued to the two FEL teams for a lower power FEL that could later be upgraded to the originally required laser power. These proposals were also reviewed and our assessment was provided to the Army SDC at WSMR in August of this year. Due to the competitive nature of the procurement, the details of our assessment will not be reported here.

4.0 SBFEL PROGRAM

SDIO's Space-based FEL program has been managed partly by the Office of Naval Research (ONR) and partly by the Army SDC at Huntsville. As part of cross-fertilization of technologies, we have undertaken to find out the significant advancements that have taken place in the SBFEL program that might have symbiotic relationship to the GBFEL. With that in mind we review below the salient SBFEL programs.

The Office of Naval Research initiated a major long term contract with TRW to design, fabricate and test key components required for an efficient high power FEL employing a superconducting accelerator as an electron beam source. The TRW SBFEL system is based on a superconducting CW accelerator with same-cell energy recovery and would use an oscillator configuration. This choice is based on their projection that this system can meet the SBFEL mission requirements. Figure 14 shows the schematic of the TRW concept of the SBFEL system. TRW is relying on a proprietary resonator design which would allow the use of very long resonators to reduce the optical flux on the mirrors. They also plan to investigate the use of gas optics and diamond lenses to reduce the required resonator length to be consistent with the space environment limitations. TRW's reasonings behind their choice of the superconducting accelerator structures are that (a) they mitigate the thermal management problem which are considered to be severe for the room temperature and cryogenic accelerators, (b) they reduce the on-board mass requirements for coolant and fuel, and (c) they are closest to demonstrating the average current capability. This last assertion is made on the strength of TRW's belief that the room temperature linacs will be limited in their current capability by the cumulative beam break-up while superconducting structures operating at higher gradients will have a much higher threshold for beam break-up. While it is true that the BBU threshold current scales with the gradient in the accelerator what is important is the average gradient (the so called 'Real Estate' gradient). In the proposed TRW's design the Real Estate Gradient is not much different than what one finds in other accelerator designs and it is therefore not clear whether there are any significant advantages to the SC design. A key feature of the TRW design is that the current pulse from the injector is fairly long occupying about 18° of RF phase angle. Due to the sinusoidal nature of the RF field, this would normally

Component Technologies for Superconducting High Power RF FEL

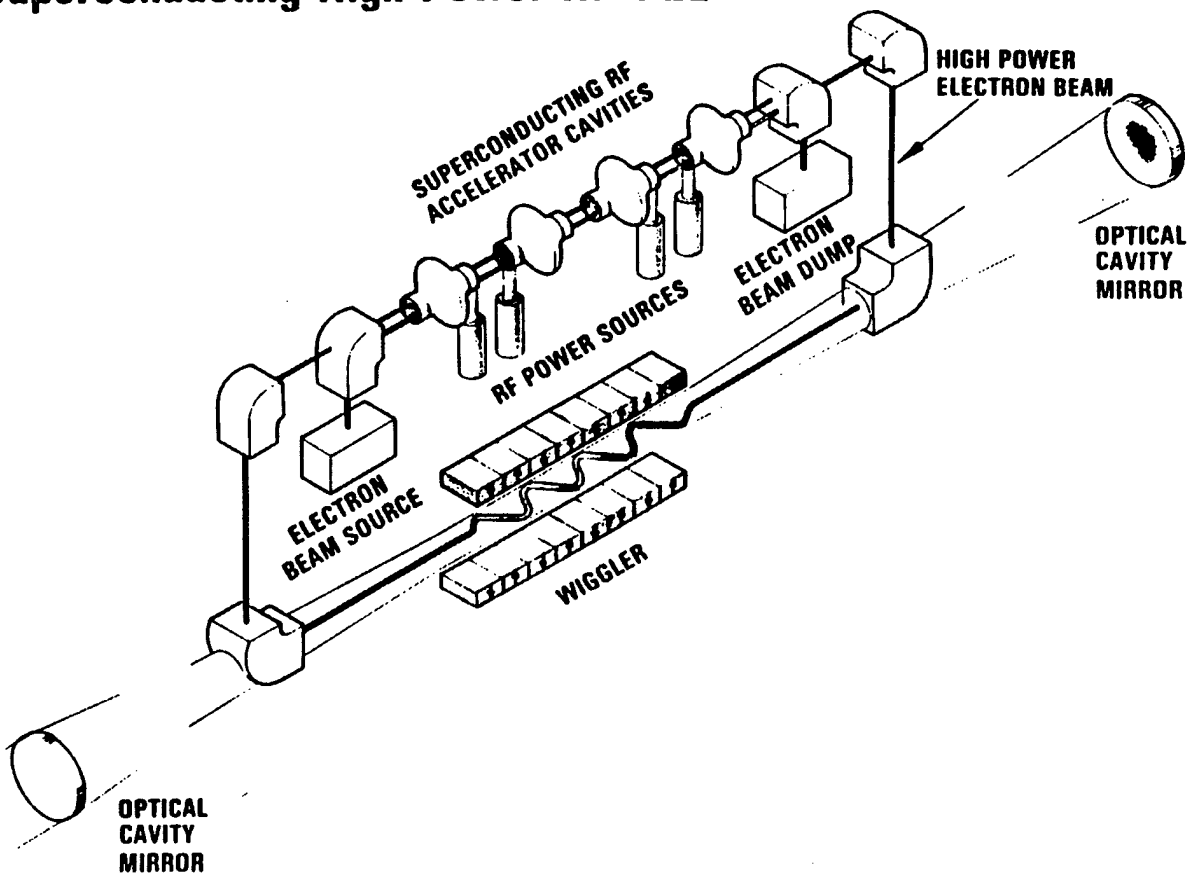

FIG. 14. SCHEMATIC OF TRW'S CONCEPT OF SUPERCONDUCTING RFLFEL FOR A SPACE-BASED LASER.

yield an energy spread (correlated) of more than 1%. To reduce the energy spread, TRW proposes to use third harmonic structures interleaved between the fundamental structures which are phased to yield a better approximation to a square wave at the crest (see Fig. 15). The peak current can therefore be lower in the linac while the charge per bunch can still be substantial. The micropulse is magnetically bunched at the end of the accelerator to increase the peak current for improved FEL performance. The use of the harmonic structures lowers the effective field gradient used in the fundamental accelerating structures. Another problem with the superconducting cavity structure is that it is susceptible to exciting higher order transverse modes that tend to deflect the beam off axis. To keep these higher order modes (HOM) from growing to unacceptable levels, HOM couplers are used that essentially take the power that is in these modes out of the cavity. The HOM couplers also take real estate which tends to decrease the average gradient. TRW's design of the 150 MeV Accelerator/Decelerator shows an overall length of ~90 meters giving an effective field gradient of ~1.5 MV/m while the peak field in the cavity is 13 MV/m. It would therefore seem that most of the advantages of using the superconducting accelerator structure to generate the high field gradients would be lost as far as the cumulative beam break-up is concerned.

One of the problems associated with using superconducting structures is the limitation on the performance of high power input couplers. Room temperature couplers are usually capable of handling 5 to 10 times more power than superconducting couplers and this might eventually limit the scalability of the superconducting linac FELs.

Since TRW plans to do energy recovery in the same accelerator cell, the average current through the accelerator essentially doubles. This has the effect of reducing the threshold BBU current. TRW does have a clever plan of debunching the beam after its passage through the wiggler and phasing them properly in the decelerator such that the electrons with most energy enter the decelerator at 180° phase angle while those with lesser energy arrive into the cavity at a lesser phase angle. This will result in the high energy electrons losing more of their energy to the rf field compared to the electrons that have already lost a good fraction of their energy in the wiggler. If the design is done correctly, one can decelerate the beam farther

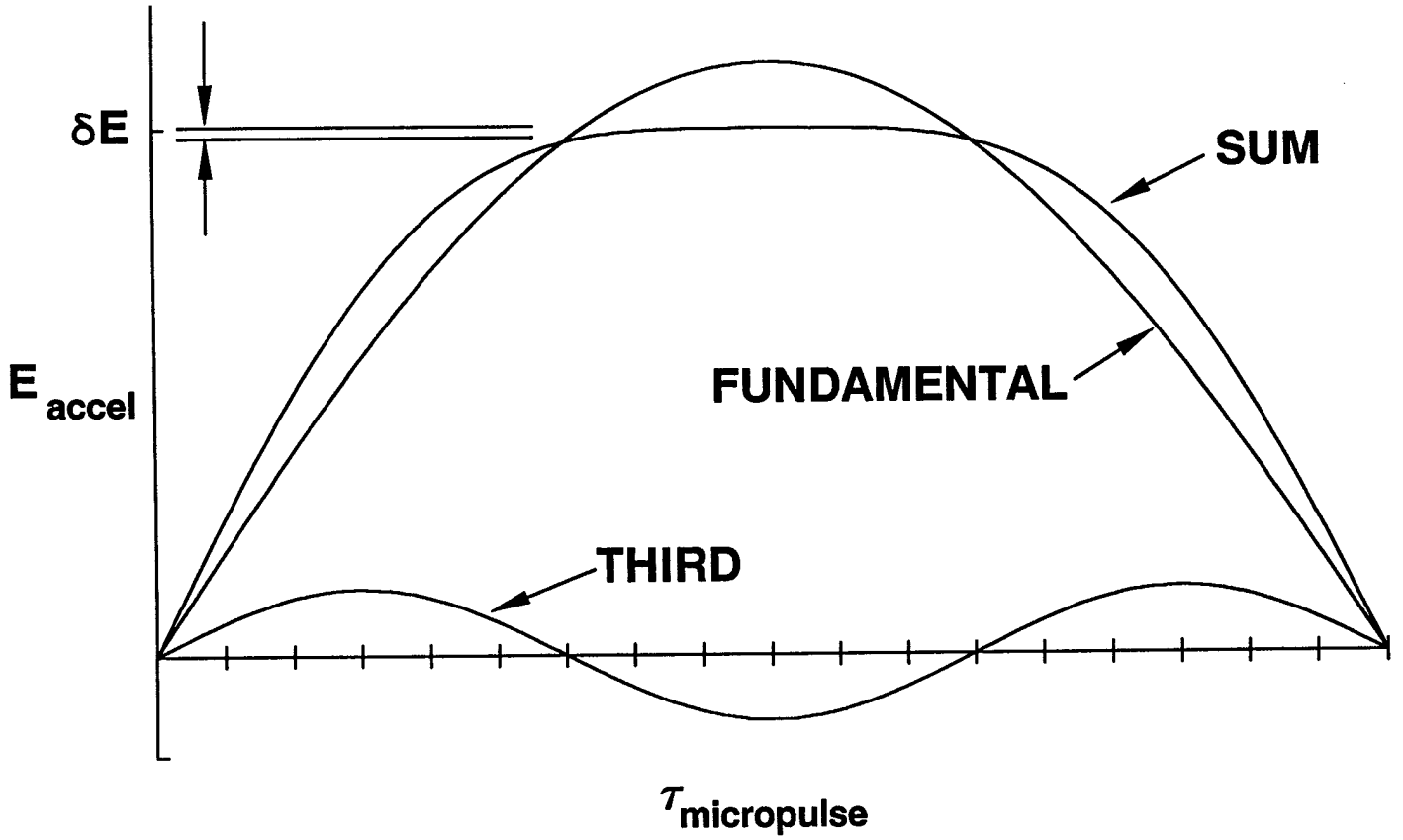

FIG. 15. PRINCIPLE OF HARMONIC COMPENSATION SHOWING THE SMALLER ENERGY SPREAD AND LONGER MICRO-PULSE LENGTH POSSIBLE.

in energy than if one did not correlate the electron energy with its arrival phase angle into the cavity. This is schematically illustrated in Fig. 16.

Experimentally, TRW has assembled the high voltage electron gun. Preliminary measurements of emittance have been carried out at 100 kV. They still have not placed any order for the superconducting cavities because of funding limitations. Energy recovery will not be attempted, another casualty to the budget constraints. TRW is also looking into advanced superconducting cavities. Materials of interest are Nb film on copper substrate and Nb_3Sn film on copper substrate. Although use of these materials is not essential for demonstrating the SBFEL system, it could lead to a simpler and more reliable system. Since copper has a much higher thermal conductivity than niobium, a system using copper substrate would allow for better heat removal and possibly higher gradient operation. Use of Nb_3Sn would permit the operation of the accelerator system at 10° K instead of 4° K. This would lead to a greatly simplified cooling system. TRW is presently suggesting that the SBFEL accelerator should operate at 100 MHz permitting the beam pipe opening to be large which will help in increasing the BBU threshold current. Other SBFEL system constructs advocate frequency of operation of the linac at 500 MHz or greater. Since the weight of the structure scales as the cube of the RF wavelength, it appears that the 100 MHz system would be far heavier than the 500 MHz system.

In FY88 ONR established a contract with Physics International (PI) to theoretically and experimentally determine the feasibility of a novel compact linear induction accelerator driving a very high power RF cavity which in turn would be used to drive a very high gradient RF Linac to be used as an electron beam source for an FEL amplifier. The PI effort has so far been limited to a paper study only due to funding limitations. The technical approach of the PI concept is shown in Figs. 17 and 18. A compact linear induction accelerator generates 0.5 MeV electron beam which is sent through a series of bunching and power extraction RF cavities. The power taken out of the electron beam by the RF cavities is replenished by induction cells interspersed in between the power extraction cavities. This RF power is fed into the High Current RF (HCRF) accelerator that consists of a photocathode injector. The gradient envisaged in the HCRF accelerator is $\approx$ 50 MV/m with a 'Real-Estate' gradient of 20 to 30 MV/m. The high current pulse then goes

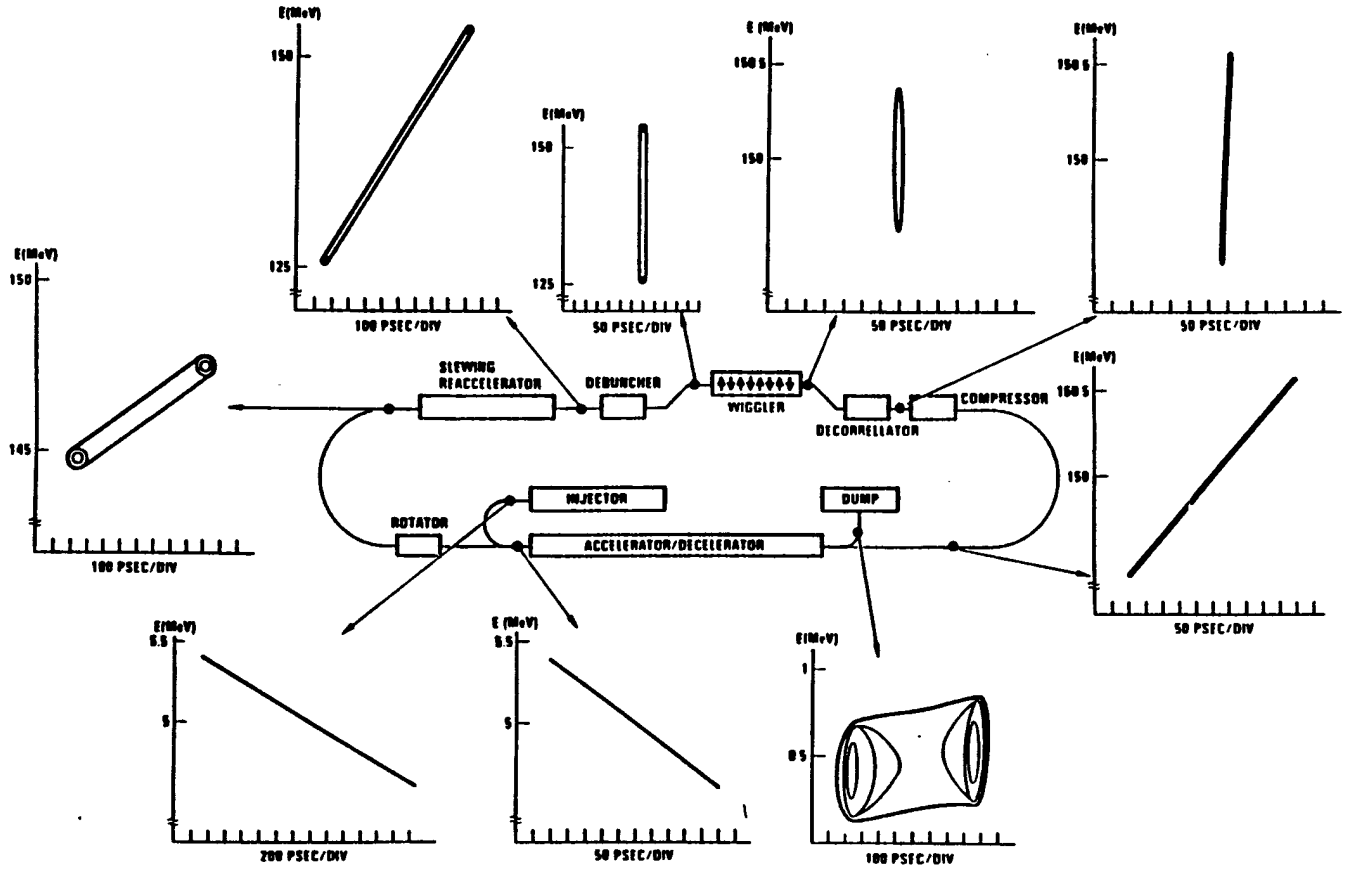

FIG. 16. TRW'S SCHEME FOR CAREFUL PHASE SPACE CONTROL AND NEAR PERFECT ENERGY RECOVERY.

- Robust and Compact Accelerator

  Drive an ambient temperature standing-wave rf accelerator structure with very high peak power (multi-GW) microwave sources to achieve high gradients (~ 20 MeV/m)

- MOPA FEL Configuration

  Use a multi-kiloamp electron beam pulse to enable high gain, single pass, master oscillator power amplifier (MOPA) FEL technology deployment

- Efficient System

  Use high beam loading and multi-microsecond rf pulses along with an optimized power train and energy recovery techniques to achieve high efficiency (~ 40% wall-plug-to-light)

- Near-Term Technology Spin-Offs

  Set technology goals consistent with eventual deployment in space but maximize the potential for near-term technology spin-offs (high power rf sources and pulsed power conditioning)

Olin

FIG. 17. TECHNICAL APPROACH BY PI FOR HCRF ACCELERATOR.

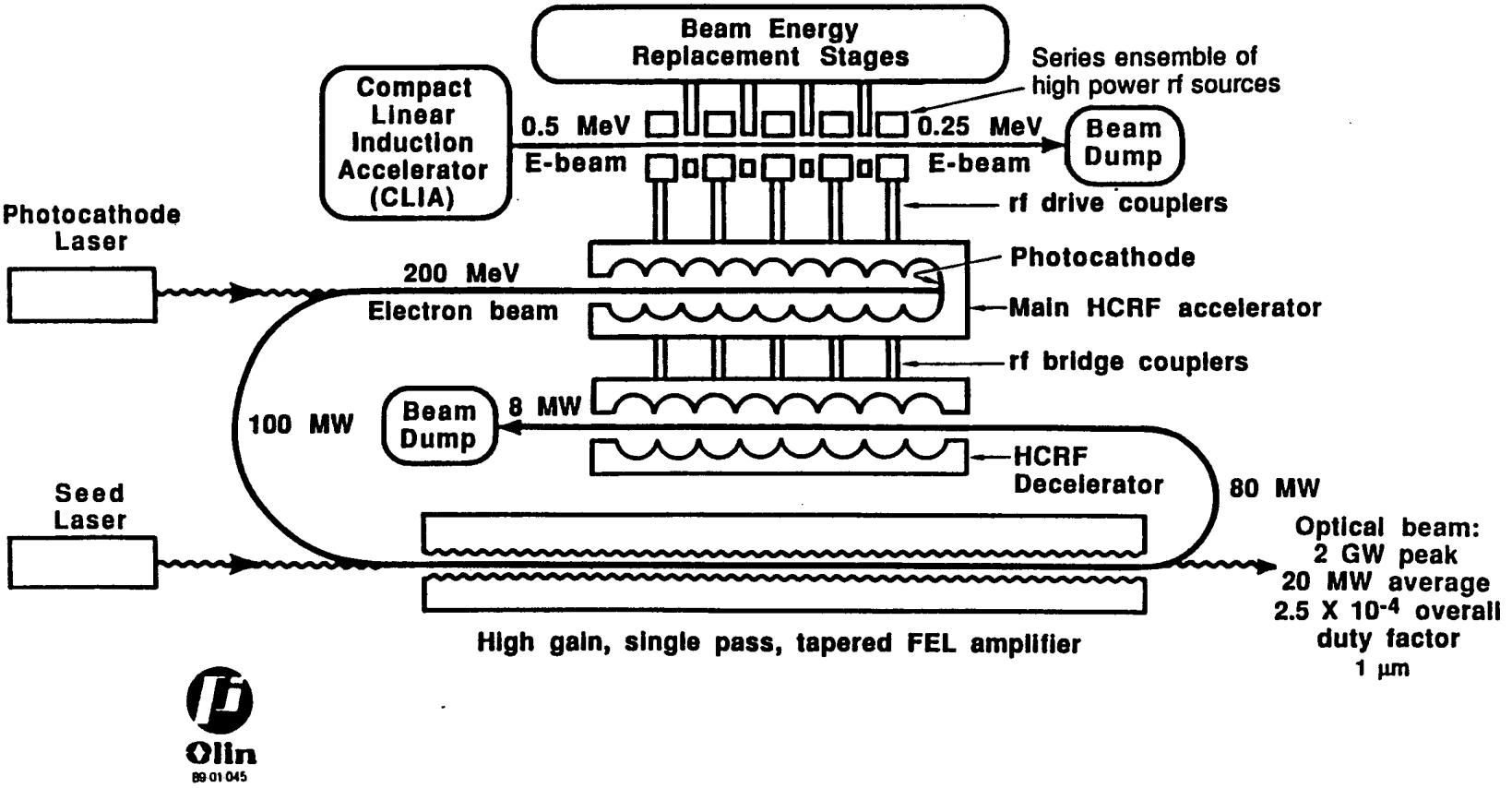

FIG. 18. SCHEMATIC OF THE HCRF ACCELERATOR BY PI.

into a tapered wiggler amplifier generating useful visible laser light output. Since the gradient in the accelerator is high, it has to be pulsed to keep the cavity wall cooling requirements manageable. Figure 19 shows the pulse format of the HCRF accelerator. PI expects an overall duty factor of 2.5×10^{-4} with macropulse lengths in the 3 to 5 μsec range. The design frequency of the SBFEL linac is 500 MHz which will have a filling time ≈ 0.5 μsec. For a reasonable overall system efficiency, one would require the pulse length be much longer than the filling time. This imposes the minimum macropulse length requirement. The current state-of-the-art of the induction accelerator is to produce 17.5 mV-sec/meter. Taking a pulse length of 5 μsec and an energy of 0.5 MeV, we find that the "Compact Linear Induction Accelerator" has to be $\approx$ 140 meters long! This, in itself, would make this concept not viable for space-basing. Figure 20 shows the efficiency goal for the overall system and individual components. Due to the pulsed nature of the system, one would expect energy droop, phase jitter, etc., which are not acceptable for achieving adequate FEL performance. Table 3 shows PI's extrapolation of the SBFEL requirements and present state-of-the-art achievements.

Another area which PI is considering is to replace the relativistic klystron with an FEL to generate the 500 MHz RF. SAIC pointed out that the wiggler parameters for such a device would be unreasonably long. In summary, the PI concept seems not very viable for scaling to high powers required for SBFEL BMD missions.

The University of Washington, under the direction of Dr. Christiansen, is pursuing work on aerolenses and gas optics. They have demonstrated the reflection of light by a gas with thermal density gradient at near glancing angle of incidence and axial aerolensing. The former application is intriguing since it allows the glancing angle incidence optics to be replaced by a wire mesh through which a hot gas flows. The fundamental radiation would be reflected off this surface, much like a mirage on a hot day. The higher harmonics, having different dispersion relationship, may either hit the screen surface or even go through the pores of the screen. It seems, therefore, to be a viable method for separating the harmonics from the fundamental in an FEL in either the oscillator or the amplifier configuration.

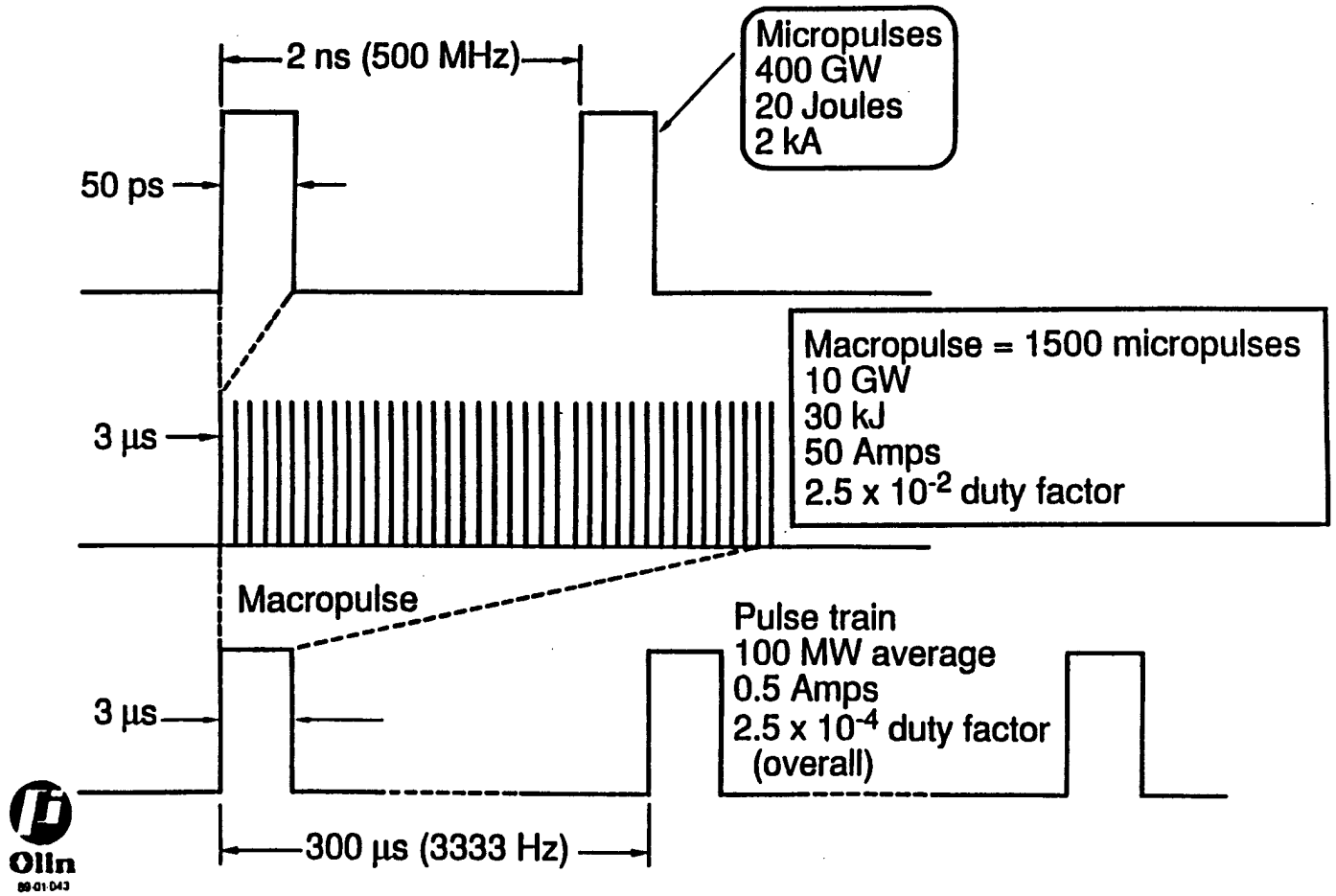

FIG. 19. THE HCRF PULSE FORMAT AS PROPOSED BY PI. THE FEL MACROPULSE LENGTH WOULD BE SHORTER BY THE FILLING TIME.

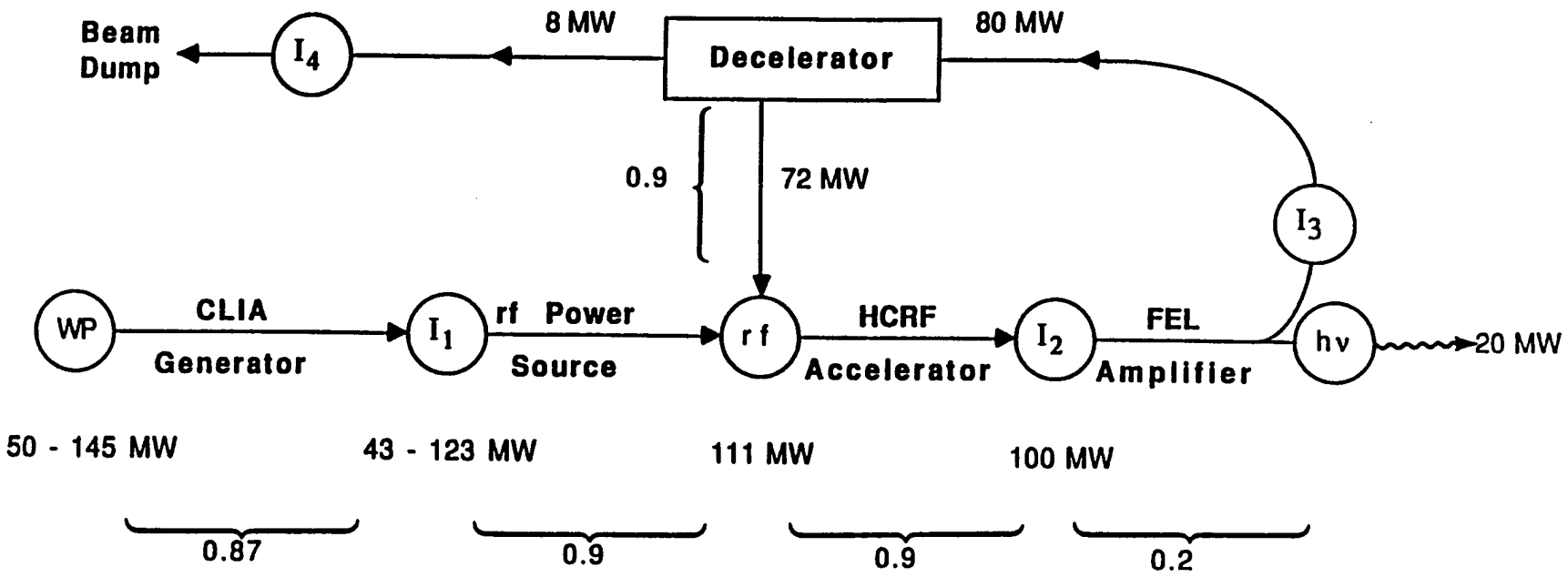

Wall-Plug-to-Light Efficiency Goal = 40 percent

FIG. 20. HCRF COMPONENT EFFICIENCY GOALS FOR SBFEL.

Table 3

REQUIREMENTS FOR THE HCRF SBFEL SYSTEM AS ENVISIONED BY PI

Selected Technology Extrapolations for Three HCRF Subsystems

Subsystem	Parameter	Brassboard Demonstrator Requirement	Far-Term SBFEL Requirement	Present State-of-the-Art*
Main Electron Accelerator	Gradient	20 MV/m	20 MV/m	5 MV/m
	Micropulse current	2 kA	2 kA	0.6-1.6 kA
	Micropulse charge	10^{-7} C	10^{-7} C	10^{-8} C
	Macropulse current	50 A	50 A	1.0 A
	Beam loading fraction	0.95	0.95	0.90
	Transverse Q	< 100	< 100	100-1000
	Wall loading	NA	350 kW/m	100-200 kW/m
	rf cycles per micropulse	1	1	
Relativistic rf Source	Frequency	500 MHz	500 MHz	1328 MHz
	Number of klystrons	10	10	1
	Peak rf power (per klystron)	1 GW	2 GW	0.5 GW
	Overall average rf power	10 GW	10 GW	0.5 GW
	Micropulses per macropulse	--	58	--
	Micropulse duration	--	30 ns	140 ns
	Macropulse duration	3.5 μs	3.5 μs	140 ns
	Electronic efficiency (per klystron)	0.5	0.5	0.4
	Overall electronic efficiency	0.9	0.9	--
	Amplitude stability	1%	1%	2%
	Phase stability	1%	1%	2%
	Macropulse repetition rate	--	3.3 kHz	--
	Lifetime	10^2	5 (10^6) shots	10^2-10^3
Relativistic Electron Beam Generator for rf Source	Electron energy	500 keV	500 keV	> 1 MeV
	Beam power per micropulse	2 GW	4 GW	> 10 GW
	Short pulse repetition rate	NA	20-30 MHz	10 MHz
	Short pulse duration	NA	30-50 ns	50 ns
	Long pulse repetition rate	3.3 kHz	3.3 kHz	5 kHz
	Long pulse duration	3.5 μs	3.5 μs	3 μs

*Not all state-of-the-art parameters achieved simultaneously

Olin

APPENDIX A

Memorandum written by Dave Quimby to Siva Mani
on FELEX code runs for comparison with FELAMP.

Date: 3 February 1989

Spectra Technology
2755 Northup Way
Bellevue, WA 98004-1495
(206) 827-0460
FAX: (206) 828-3517

To: Siva Mani

From: Dave Quimby

Subject: Induction-FEL Simulation

Enclosed are the self-design taper prescription and plots from the revised induction-FEL test case. For this run I have used :

E-BEAM
Gamma = 392.4 (E = 200 MeV)
I = 2000 A
DelGamma/Gamma = 0.1 % (Gaussian, Full Width at 1/e Points)
Normalized Edge Emit = 447 pi mm-mrad
Brightness = (2 pi**2 I)/(emit**2) = 2.E6 A/(cm-rad)**2
Edge Radius = 0.22 cm
Unif-Filled 4-Space
4096 electrons

WIGGLER
L = 100 m
B = 3.19 kG (Aw = 1.688)
Period = 8.0 cm
Curved-Pole Focus
Self Designed Taper for Constant PsiR = 20 degrees
at Radius = 0.65 Reb

OPTICAL BEAM
Lambda = 1.0 microns
Input Power = 100 MW
Rayleigh Range = 48 m
Beam waist at wiggler entrance
Waist Radius = 0.39 cm (1/e**2 intensity)

GRID
128x128 cells out to (x,y) = 1.65 cm
Axial step size = 12.5 cm

The taper is designed for the case where the wavelength of the input optical beam is precisely on resonance. Under these conditions the most remarkable result is the high sensitivity to details of the electron energy spread and emittance phase space distributions. The e-beam brightness was varied giving the following results:

Brightness	Extraction(%)	Gain (Pout/Pin)
1.0E6	9.1	370
2.0E6	24	970
4.0E6	30	1210

(For these three runs a coarse axial grid (20 cm step) was used; this accounts for the slight difference in extraction compared to the values quoted below.)

Variation of the full width of the Gaussian energy spread distribution yielded:

E-Spread (1/e FW)	Extraction(%)	Gain (Pout/Pin)
0.10 %	26.2	1050
0.25	19.9	800
0.50	14.7	590
0.75	11.9	480
1.00	8.9	360

At fixed e-beam brightness, I also found high sensitivity to the form assumed for filling the emittance phase space:

Distribution	Extraction(%)	Gain (Pout/Pin)
Uniformly-Filled	26.2	1050
Uncorrel. Gaussian	17.8	711

For the uncorrelated Gaussian case, I took the edge radius (0.22 cm) to be the radius which encloses 90 percent of the particles. (This places the resonant particle at the 1/e point, r = 0.144 cm.)

For the 1.0E6 brightness case, I scanned through possible values of PsiR and verified that 20 degrees approximately optimizes the performance. For the 2.0E6 brightness case, I fixed the taper prescription and varied the input optical wavelength:

DelLambda/Lambda	Extraction(%)
-1.50 %	18.8
-1.25	23.0
-1.00	27.7
-0.75	30.0
-0.50	30.4
-0.25	28.1
0.	26.2
0.25	23.3
0.50	16.0
0.75	4.8
1.00	0.73

Apparently the capture fraction is slightly higher under these high gain conditions when the electrons are started off slightly below resonance.

I had expected that focusing the input beam to a tighter spot size might improve performance. I tried Rayleigh range values from 12 to 96 meters, (which varies the spot size by a factor of three) but find this only makes a 10 percent difference. Furthermore the larger spot sizes give slightly better performance. (In retrospect I realize that this is because of the prebunching effect achieved by the initial exponential gain region when starting at lower optical intensities.) I have not tried varying the radius of curvature of the input beam. The accompanying plots indicate that the optical beam tries to find an asymptotic R value of about 50 m, so starting the beam with that curvature might help a little.

Best of luck with your simulation code.

cc. J. Slater

```
xfel    - a 3-d fel simulation code -  dated 4/1/87

run information for xfel
 job run under user # 802731
        on account # 9401rc61
       with dropfile +xfelem
        under suffix e
                  on 01/30/89
                  at 11:57:40 mst
             machine 2

*****************************************

optical gain and extraction efficiency,

   energy(J) in= 1.009e-03    energy(J) out= 1.058e+00

   power(W) in= 1.008e+08    power(W) out= 1.057e+11

   gain= 1.049e+03    effic(%)= 2.624e+01

   energy balance= 3.920e-03
```

SELF-DESIGN TAPER PRESCRIPTION

the wiggler parameters,

z(cm)	bfld(g)	λ_w (cm)	K ($\sqrt{2}$ a_w)	gap (cm)
-5.000e+03	3.175e+03	8.000e+00	2.372e+00	4.112e+00
-4.750e+03	3.181e+03	8.000e+00	2.376e+00	4.108e+00
-4.500e+03	3.178e+03	8.000e+00	2.374e+00	4.110e+00
-4.250e+03	3.163e+03	8.000e+00	2.363e+00	4.121e+00
-4.000e+03	3.149e+03	8.000e+00	2.352e+00	4.131e+00
-3.750e+03	3.133e+03	8.000e+00	2.340e+00	4.142e+00
-3.500e+03	3.110e+03	8.000e+00	2.323e+00	4.158e+00
-3.250e+03	3.088e+03	8.000e+00	2.307e+00	4.174e+00
-3.000e+03	3.065e+03	8.000e+00	2.289e+00	4.192e+00
-2.750e+03	3.037e+03	8.000e+00	2.269e+00	4.212e+00
-2.500e+03	3.008e+03	8.000e+00	2.247e+00	4.234e+00
-2.250e+03	2.975e+03	8.000e+00	2.223e+00	4.259e+00
-2.000e+03	2.940e+03	8.000e+00	2.196e+00	4.286e+00
-1.750e+03	2.902e+03	8.000e+00	2.168e+00	4.316e+00
-1.500e+03	2.862e+03	8.000e+00	2.138e+00	4.347e+00
-1.250e+03	2.821e+03	8.000e+00	2.107e+00	4.381e+00
-1.000e+03	2.777e+03	8.000e+00	2.074e+00	4.418e+00
-7.500e+02	2.730e+03	8.000e+00	2.040e+00	4.457e+00
-5.000e+02	2.680e+03	8.000e+00	2.002e+00	4.500e+00
-2.500e+02	2.631e+03	8.000e+00	1.965e+00	4.544e+00
-3.001e-11	2.578e+03	8.000e+00	1.926e+00	4.592e+00
2.500e+02	2.524e+03	8.000e+00	1.885e+00	4.643e+00
5.000e+02	2.469e+03	8.000e+00	1.844e+00	4.696e+00
7.500e+02	2.409e+03	8.000e+00	1.799e+00	4.755e+00
1.000e+03	2.350e+03	8.000e+00	1.755e+00	4.815e+00
1.250e+03	2.288e+03	8.000e+00	1.709e+00	4.881e+00
1.500e+03	2.225e+03	8.000e+00	1.662e+00	4.950e+00
1.750e+03	2.160e+03	8.000e+00	1.613e+00	5.025e+00
2.000e+03	2.094e+03	8.000e+00	1.564e+00	5.104e+00

```
2.250e+03  2.027e+03  8.000e+00  1.514e+00  5.187e+00
2.500e+03  1.957e+03  8.000e+00  1.462e+00  5.278e+00
2.750e+03  1.886e+03  8.000e+00  1.409e+00  5.376e+00
3.000e+03  1.814e+03  8.000e+00  1.355e+00  5.480e+00
3.250e+03  1.741e+03  8.000e+00  1.301e+00  5.591e+00
3.500e+03  1.667e+03  8.000e+00  1.246e+00  5.711e+00
3.750e+03  1.592e+03  8.000e+00  1.189e+00  5.841e+00
4.000e+03  1.517e+03  8.000e+00  1.133e+00  5.980e+00
4.250e+03  1.440e+03  8.000e+00  1.076e+00  6.135e+00
4.500e+03  1.363e+03  8.000e+00  1.018e+00  6.301e+00
4.750e+03  1.286e+03  8.000e+00  9.604e-01  6.484e+00
5.000e+03  1.208e+03  8.000e+00  9.023e-01  6.686e+00

cpu(sec)= 0.647e+02   io(sec)= 0.116e+02   sys(sec)= 0.708e+00
```

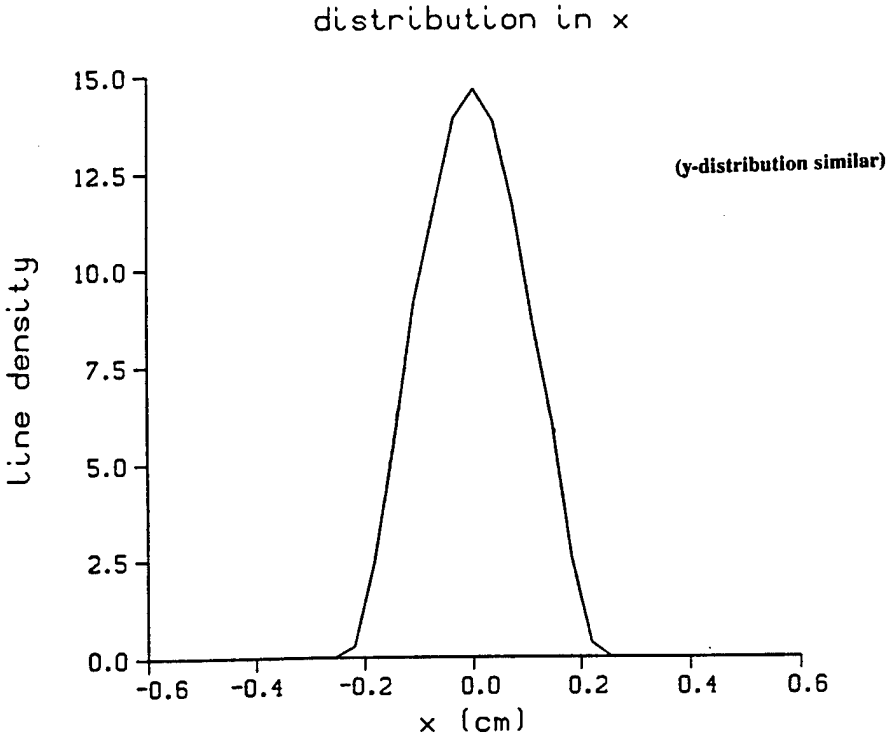
distribution in x
15.0
12.5
10.0
7.5
5.0
2.5
0.0
Line density
-0.6
-0.4
-0.2
0.0
0.2
0.4
0.6
x (cm)
(y-distribution similar)

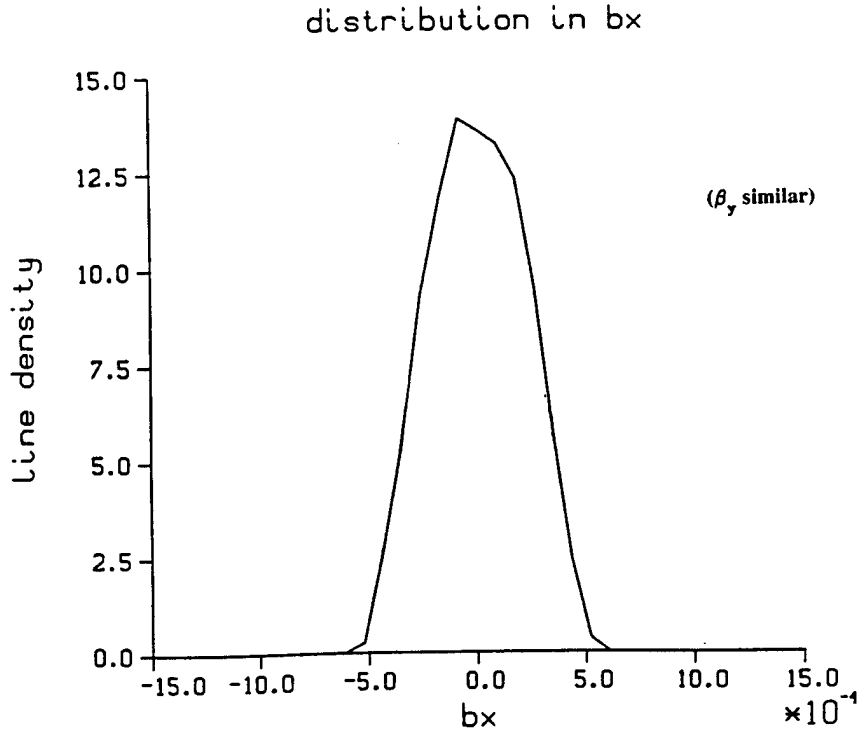
distribution in bx
15.0
12.5
10.0
7.5
5.0
2.5
0.0
Line density
-15.0
-10.0
-5.0
0.0
5.0
10.0
15.0
bx
×10⁻⁴
(β_y similar)

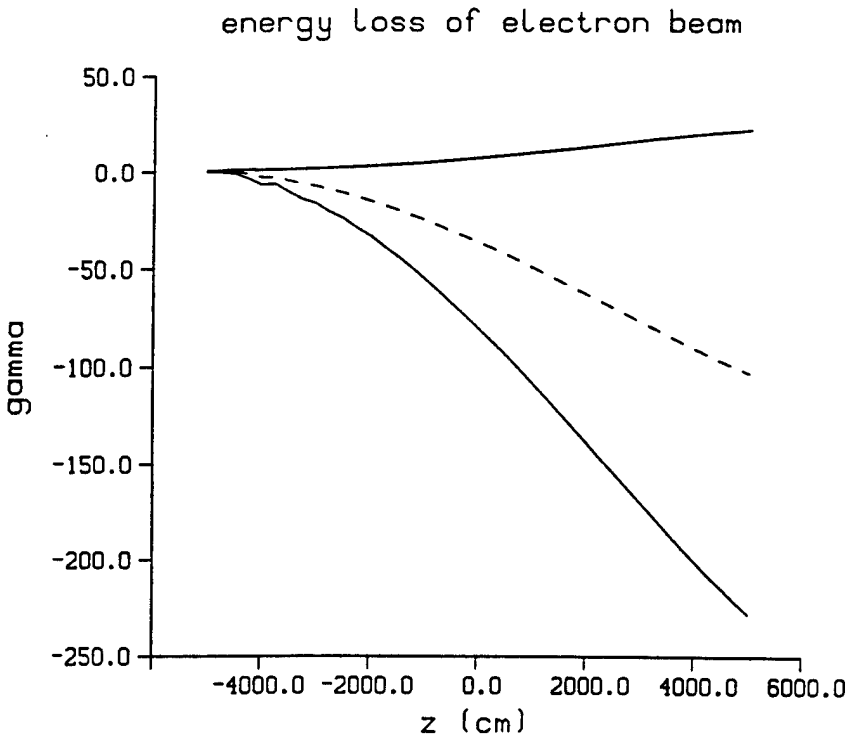
energy loss of electron beam
50.0
0.0
-50.0
-100.0
-150.0
-200.0
-250.0
gamma
-4000.0
-2000.0
0.0
2000.0
4000.0
6000.0
z (cm)

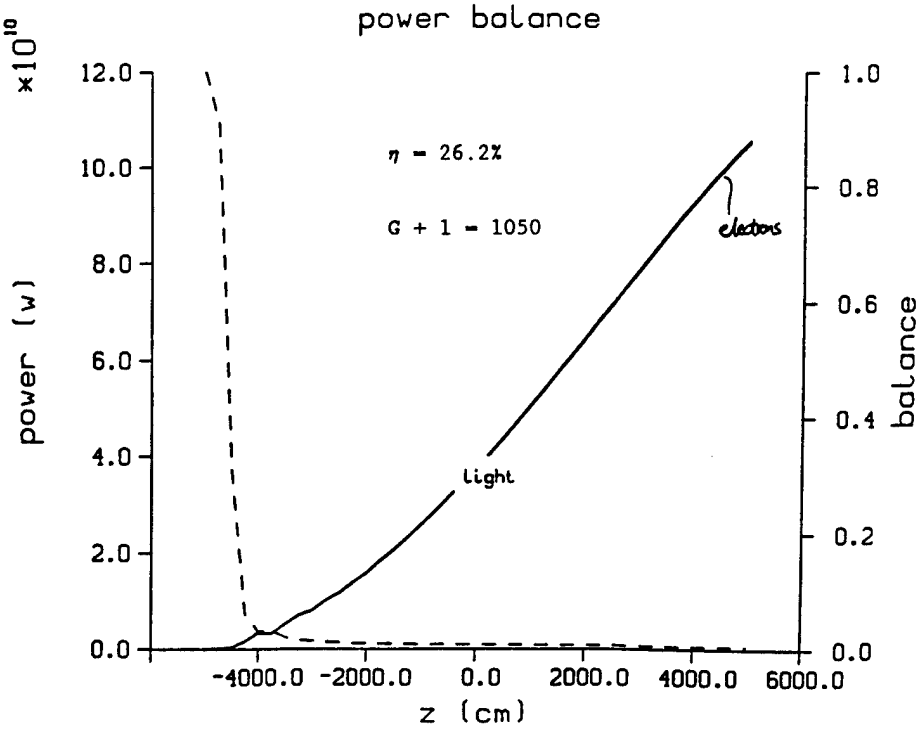
power balance
*10^10
12.0
10.0
8.0
6.0
4.0
2.0
0.0
power (w)
η = 26.2%
G + 1 = 1050
electrons
light
1.0
0.8
0.6
0.4
0.2
0.0
balance
-4000.0
-2000.0
0.0
2000.0
4000.0
6000.0
z (cm)

size of electron beam

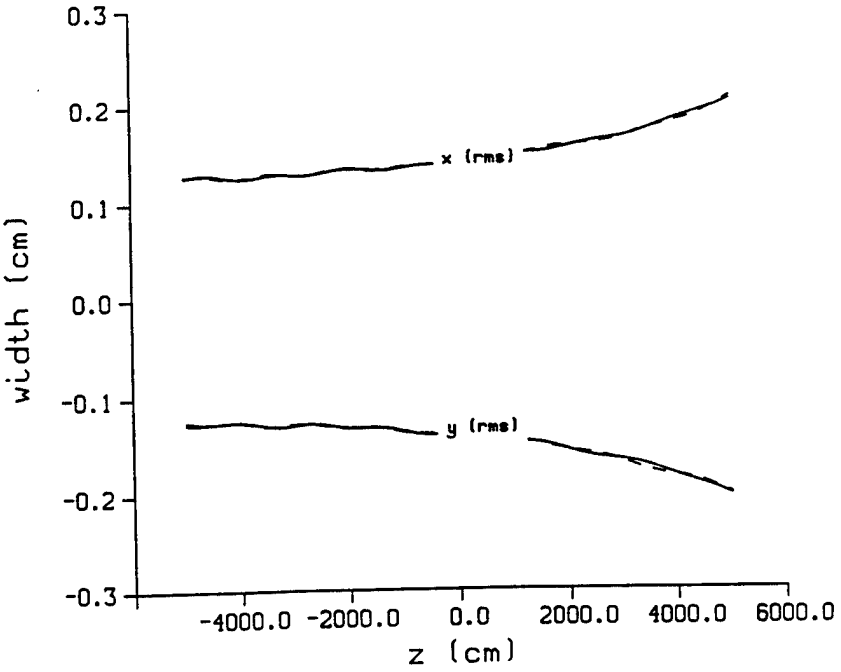

beta spread of electron beam

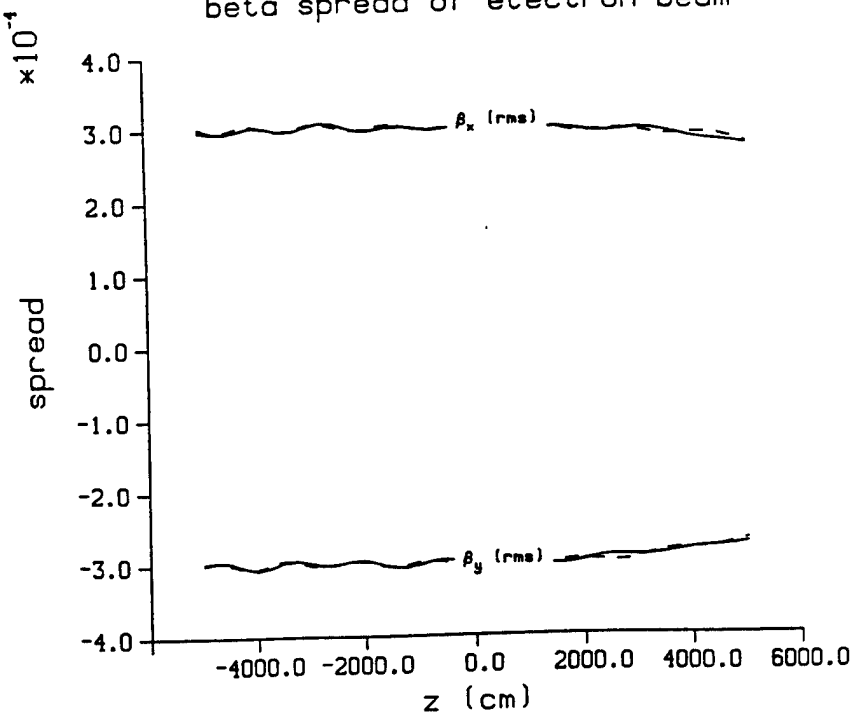

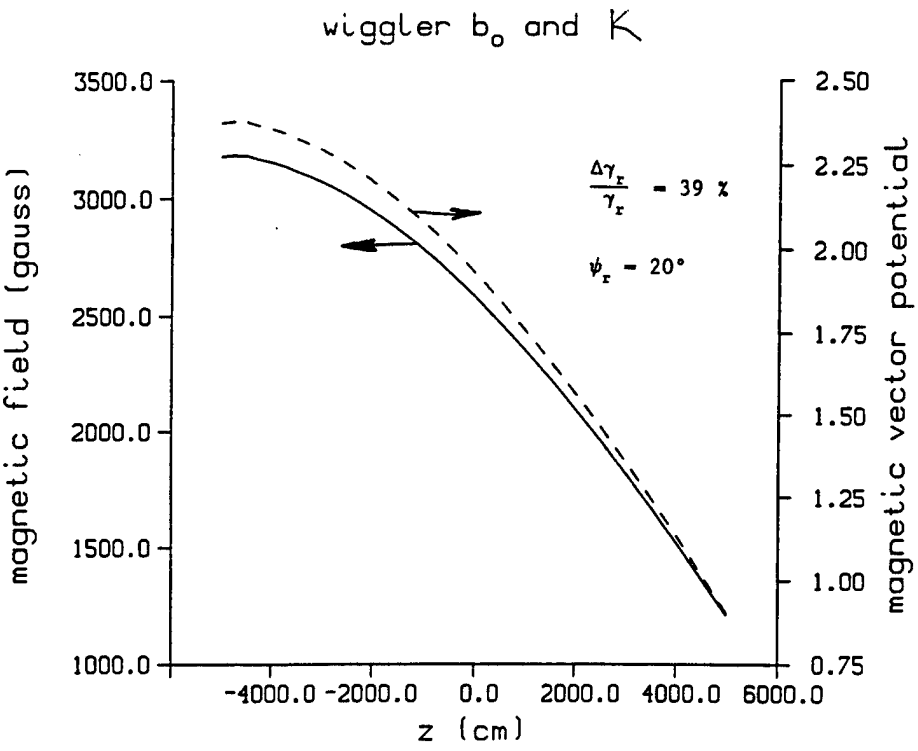
wiggler b_o and K
magnetic field (gauss)
magnetic vector potential
z (cm)
3500.0
3000.0
2500.0
2000.0
1500.0
1000.0
2.50
2.25
2.00
1.75
1.50
1.25
1.00
0.75
-4000.0 -2000.0 0.0 2000.0 4000.0 6000.0
$\frac{\Delta\gamma_r}{\gamma_r}$ = 39 %
ψ_r = 20°

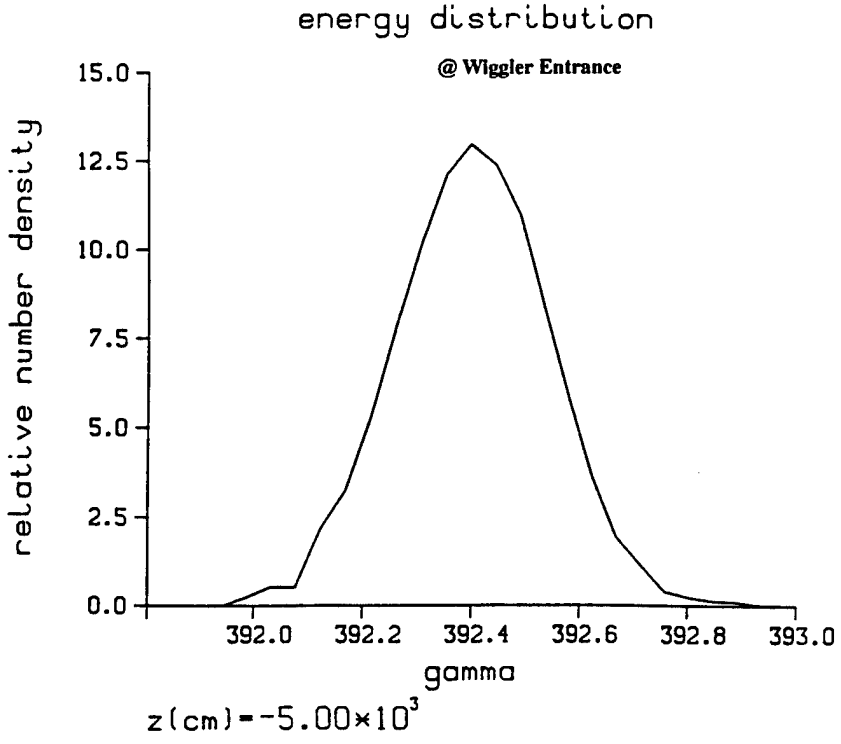
energy distribution
@ Wiggler Entrance
relative number density
gamma
15.0
12.5
10.0
7.5
5.0
2.5
0.0
392.0 392.2 392.4 392.6 392.8 393.0
z(cm)=-5.00×10³

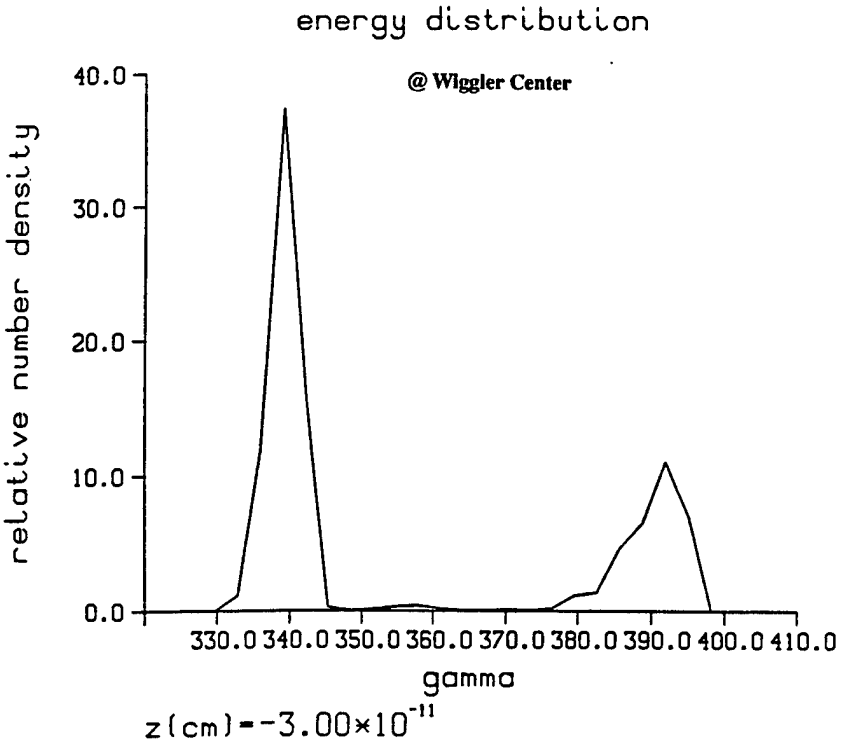
energy distribution
@ Wiggler Center
relative number density
40.0
30.0
20.0
10.0
0.0
330.0 340.0 350.0 360.0 370.0 380.0 390.0 400.0 410.0
gamma
z(cm)=-3.00×10^-11

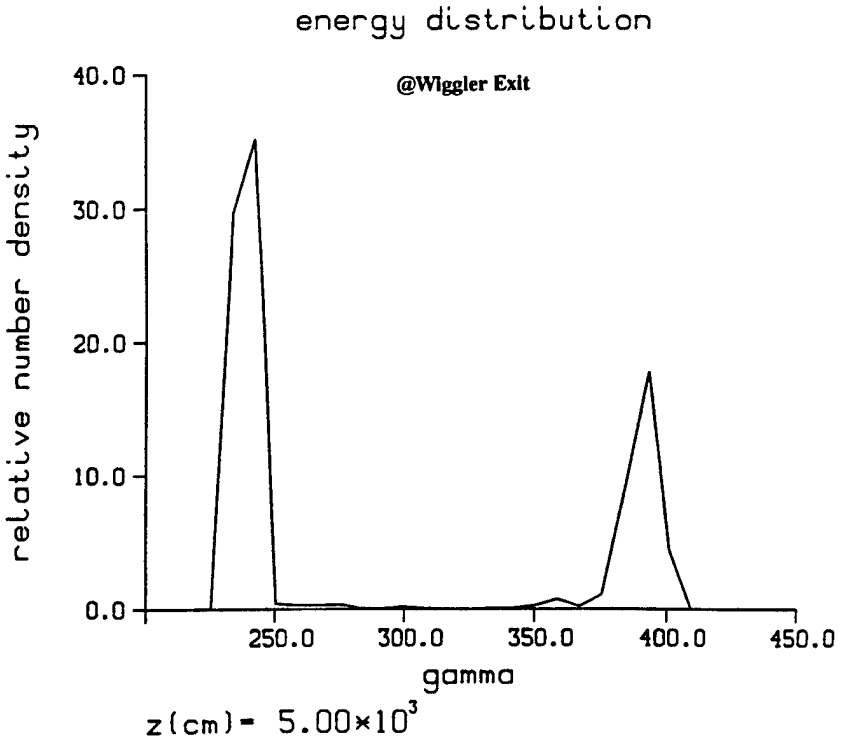
energy distribution
@Wiggler Exit
relative number density
40.0
30.0
20.0
10.0
0.0
250.0 300.0 350.0 400.0 450.0
gamma
z(cm)= 5.00×10^3

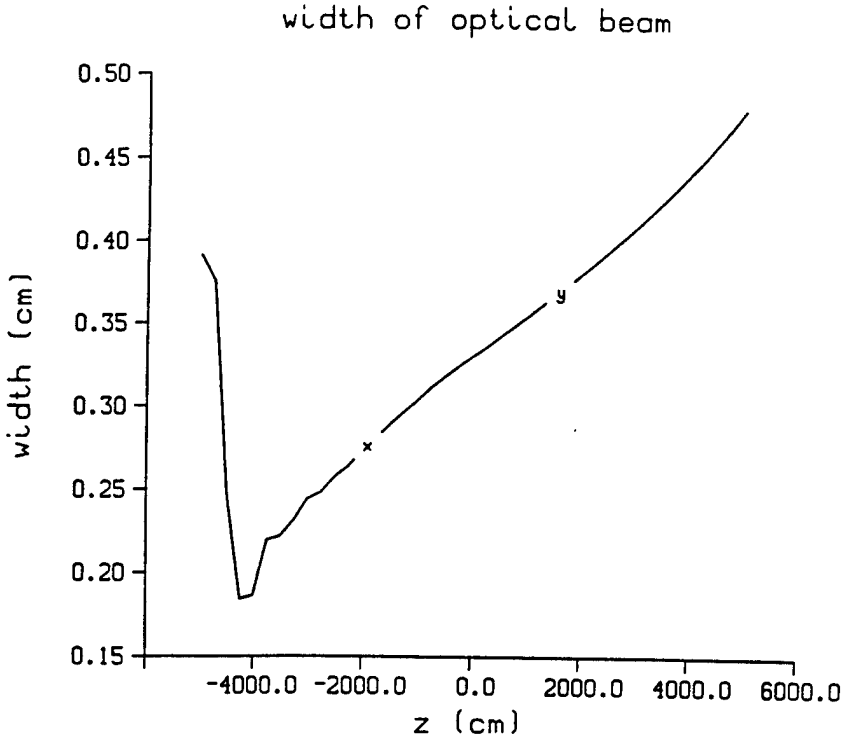
width of optical beam
0.50
0.45
0.40
0.35
0.30
0.25
0.20
0.15
width (cm)
x
y
-4000.0
-2000.0
0.0
2000.0
4000.0
6000.0
z (cm)

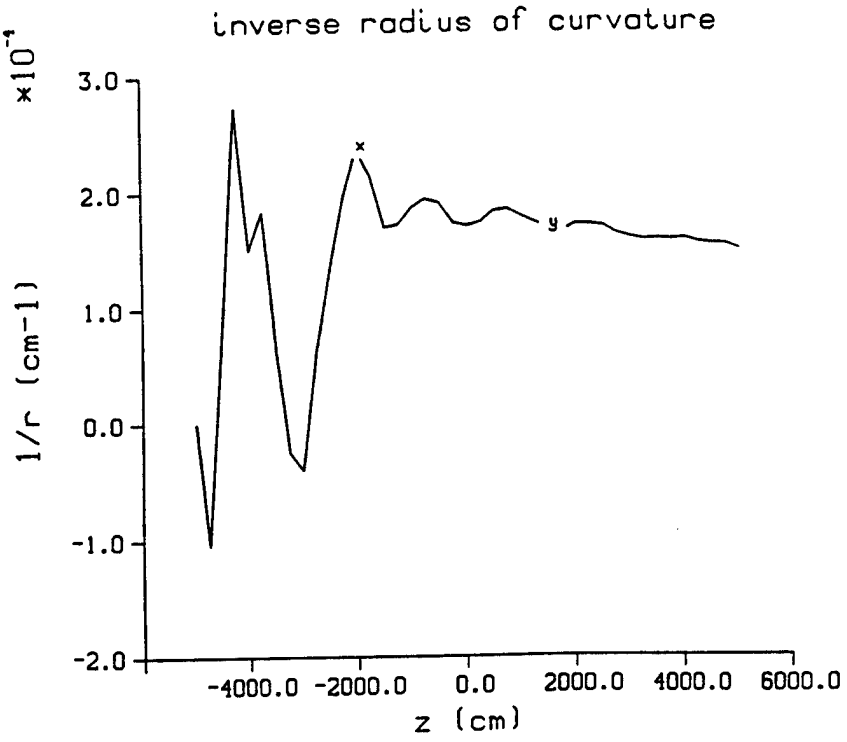
inverse radius of curvature
x10⁻¹
3.0
2.0
1.0
0.0
-1.0
-2.0
1/r (cm-1)
x
y
-4000.0
-2000.0
0.0
2000.0
4000.0
6000.0
z (cm)

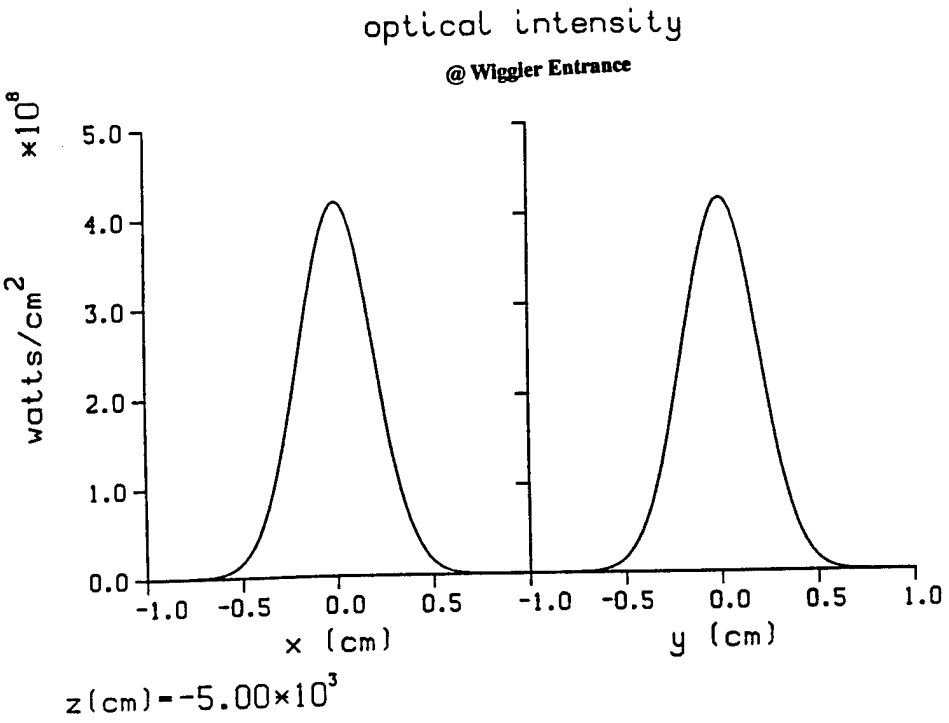
optical intensity
@ Wiggler Entrance
watts/cm^2 ×10^8
5.0
4.0
3.0
2.0
1.0
0.0
-1.0 -0.5 0.0 0.5
x (cm)
-1.0 -0.5 0.0 0.5 1.0
y (cm)
z(cm)=-5.00×10^3

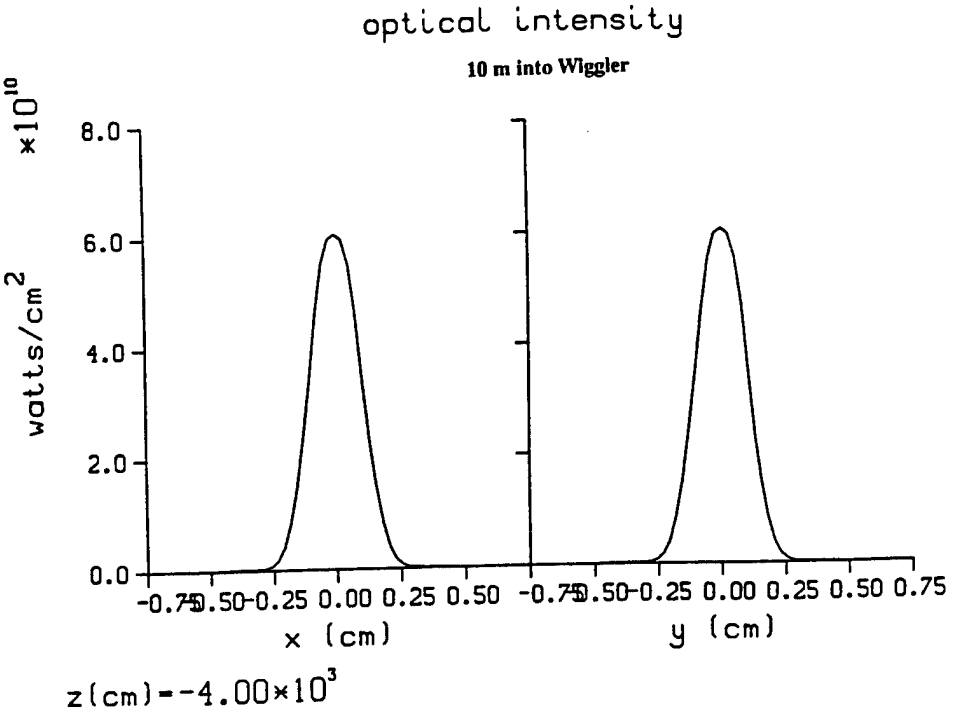
optical intensity
10 m into Wiggler
watts/cm^2 ×10^{10}
8.0
6.0
4.0
2.0
0.0
-0.75 -0.50 -0.25 0.00 0.25 0.50
x (cm)
-0.75 -0.50 -0.25 0.00 0.25 0.50 0.75
y (cm)
z(cm)=-4.00×10^3

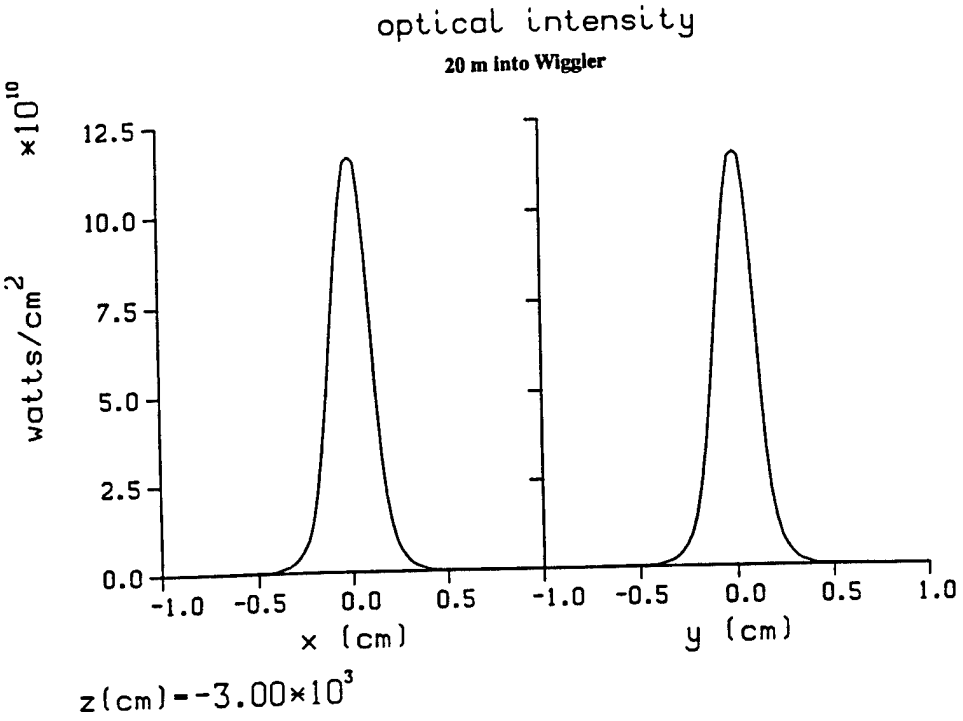
optical intensity
20 m into Wiggler
watts/cm^2 ×10^{10}
12.5
10.0
7.5
5.0
2.5
0.0
-1.0 -0.5 0.0 0.5
x (cm)
-1.0 -0.5 0.0 0.5 1.0
y (cm)
z(cm)=-3.00×10^3

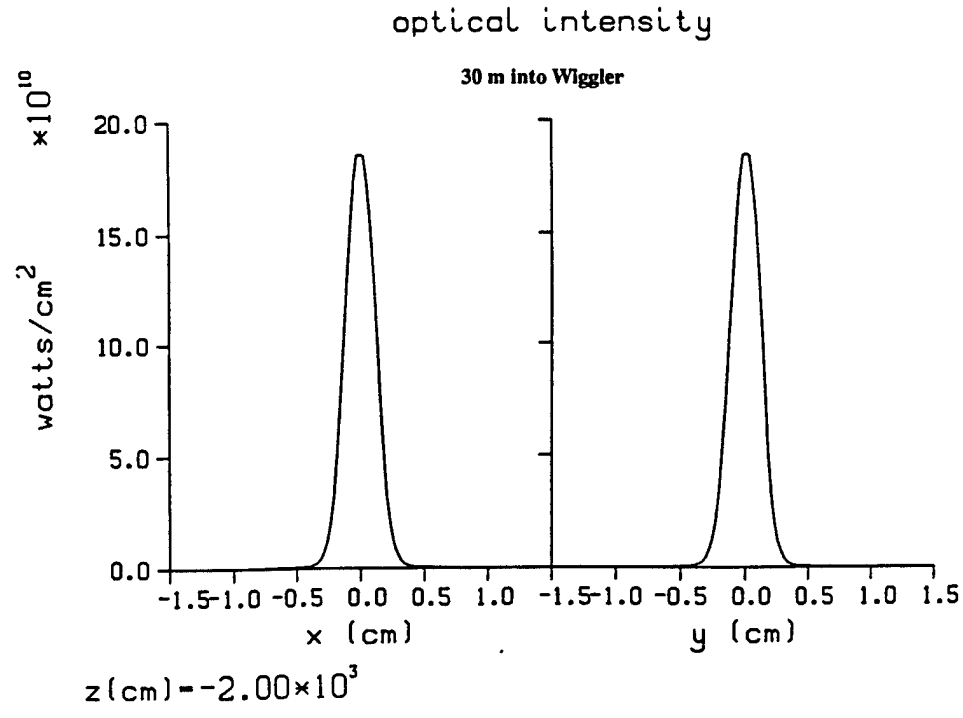
optical intensity
30 m into Wiggler
watts/cm^2 ×10^{10}
20.0
15.0
10.0
5.0
0.0
-1.5-1.0 -0.5 0.0 0.5 1.0
x (cm)
-1.5-1.0 -0.5 0.0 0.5 1.0 1.5
y (cm)
z(cm)=-2.00×10^3

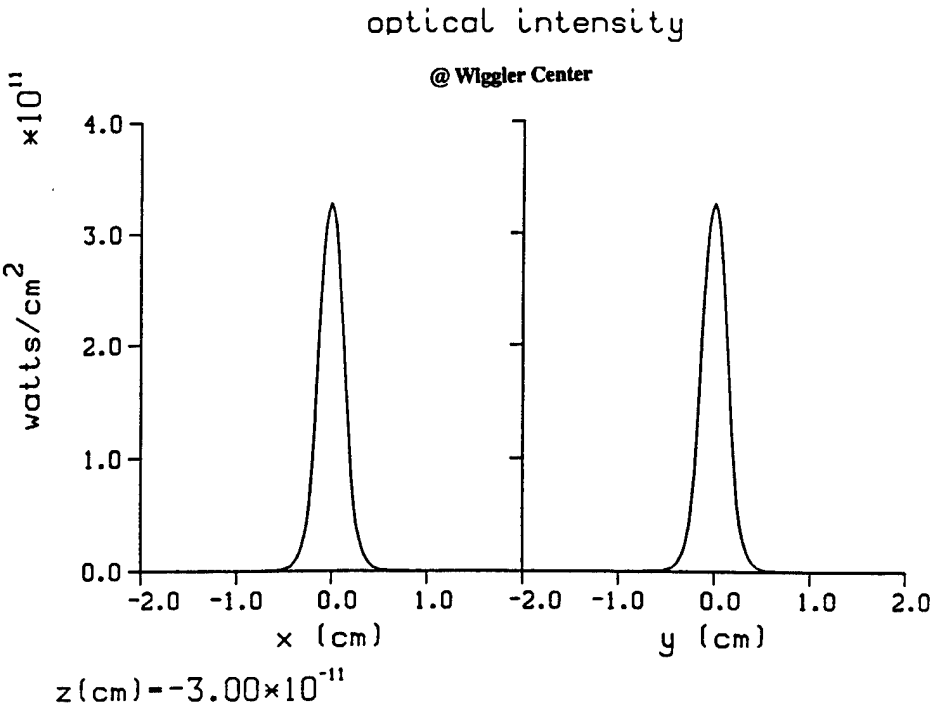
optical intensity
@ Wiggler Center
watts/cm2
*10^11
4.0
3.0
2.0
1.0
0.0
-2.0 -1.0 0.0 1.0
x (cm)
-2.0 -1.0 0.0 1.0 2.0
y (cm)
z(cm)=-3.00*10^-11

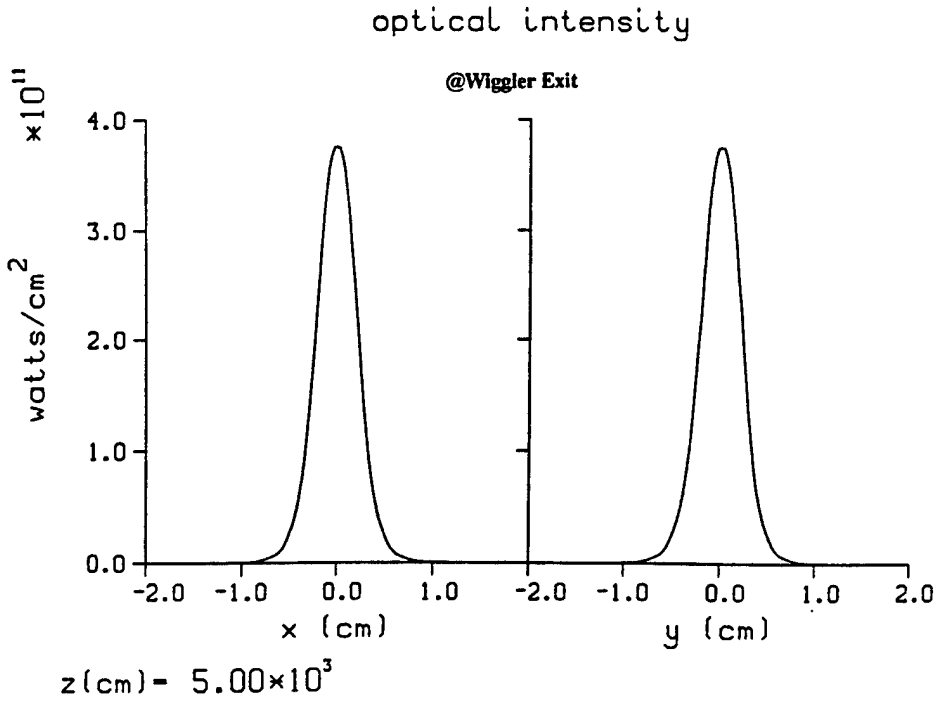
optical intensity
@Wiggler Exit
watts/cm2
*10^11
4.0
3.0
2.0
1.0
0.0
-2.0 -1.0 0.0 1.0
x (cm)
-2.0 -1.0 0.0 1.0 2.0
y (cm)
z(cm)= 5.00*10^3

REFERENCES

1. G. Bourianoff, J. Long, and S. A. Mani, "Space Based Directed Energy Technology Support - Technical Area I: Analysis of Free Electron Lasers for Strategic Defense," to U.S. Army Micom Directed Energy Directorate under Contract No. DAAH01-86-D-0007, Delivery Order No. 21, Vol. 1, 30 September 1988.

2. E. T. Scharlemann, J. Appl. Phys. 58, 2154 (1985).

3. R. L. Tokar, B. D. VcVey, L. E. Thode, and G. M. Gallatin, IEEE J. Quant. Elec., Vol. QE-25, 73 (1989).

4. W. B. Colson and S. K. Ride, *Free Electron Generators of Coherent Radiation*, Physics of Quantum Electronics, Vol. 7, S.F. Jacobs et al. Eds., Reading, MA, Addison-Wesley, 1980, p.377.

5. Dave Quimby, Private Communication (1989). [See Appendix].

6. S. A. Mani, *Free Electron Generators of Coherent Radiation*, Physics of Quantum Electronics, Vol. 7, S. F. Jacobs et al. Eds., Reading, MA, Addison-Wesley, 1980, p. 589.